University of Alberta

Functional studies on the human sodium proton exchanger isoform 1

by

Jennifer Tzeng

A thesis submitted to the Faculty of Graduate Studies and Research
in partial fulfillment of the requirements for the degree of

Master of Science

Biochemistry

© Jennifer Tzeng
Spring 2011
Edmonton, Alberta

Permission is hereby granted to the University of Alberta Libraries to reproduce single copies of this thesis and to lend or sell such copies for private, scholarly or scientific research purposes only. Where the thesis is converted to, or otherwise made available in digital form, the University of Alberta will advise potential users of the thesis of these terms.

The author reserves all other publication and other rights in association with the copyright in the thesis and, except as herein before provided, neither the thesis nor any substantial portion thereof may be printed or otherwise reproduced in any material form whatsoever without the author's prior written permission.

Examining Committee

Dr. Larry Fliegel, Biochemistry

Dr. Brian Sykes, Biochemistry

Dr. Joe Casey, Physiology

Dedication

To my family: Winston, Chen-Hui, Roger, and Lance.

Abstract

The mammalian Na^+/H^+ exchanger isoform 1 (NHE1) is a ubiquitous membrane protein that exchanges one intracellular H^+ for an extracellular Na^+, thereby regulating cell pH and volume. NHE1 catalytic activity is mediated by a transmembrane (TM) domain with 12 transmembrane segments. We performed cysteine scanning mutagenesis on TMVI (Asn227–Ile249) of NHE1. Each residue of TMVI was mutated into a cysteine in the background of a cysteineless NHE1 protein. MTSET and MTSES are sulfhydryl reactive membrane impermeable compounds able to react with accessible cysteines. Asp238Cys, Pro239Cys, and Glu247Cys expressed inactive NHE1. Asn227Cys, Ile233Cys, and Leu243Cys were strongly inhibited by MTSET, suggesting their pore lining properties. More mutations were introduced to characterize critical residues in TMVI. The Glu248Gln and Leu243Ala mutants were more susceptible to limited proteolytic attack by trypsin suggesting an altered conformation. The results suggest that Glu248 and Leu243 are important in protein structure, stability, and folding.

Acknowledgement

I want to thank my supervisor Dr. Larry Fliegel for his guidance and instruction throughout my masters program. I really appreciate all the help from my lab members especially Xiuju and Yong. And I thank everyone in the department of Biochemistry, who showed friendliness, shared knowledge and provided suggestions during my study. I also thank my committee members Dr. Brian Sykes and Dr. Joe Casey for being very insightful towards my research. I want to mention Brian Lee, a PhD student in Dr. Sykes lab, who performed NMR studies on NHE1 TMVI. Lastly, I am very grateful to be able to complete my Masters degree at the University of Alberta.

Table of Contents

List of Tables

List of Figures

Abbreviations

α-MEM	Modified Eagle's medium, α-modification
12CA5	Anti-HA antibody
Amiloride	3,5 diamino-6-chloro-N-(diaminomethylene)pyrazinecardoxamide
Amp	Ampicillin
Ang II	Angiotensin-II
AP1	Chinese hamster ovary cell line deficient in plasma membrane Na^+/H^+ exchanger
ATP	Adenosine 5'-triphosphate
BCECF	2'-7'-bis(2-carboxyethyl)-5(6)-carboxyfluorescein
BCECF-AM	2'-7'-bis(2-carboxyethyl)-5(6)-carboxyfluorescein acetoxy methyl ester
BGS	Bovine growth serum
bp	base pair
CAII	Carbonic anhydrase II
CaM	Calmodulin
cDNA	Complementary deoxyribonucleic acid
CHP1	Calcineurin B homologous protein isoform 1
CHO	Chinese hamster ovary cell line
C-terminal	Carboxy terminal
DIDS	4,4'-diisothiocyanostilbene-2,2'-disulfonic acid
DMA	5-(N,N-dimethyl) amiloride
DNA	Deoxyribonucleic acid
dNTP	Deoxyribonucleoside triphosphate
DPC	Dodecylphosphocholine
ECL	Enhanced Chemiluminescence
EcNhaA	E. Coli Na^+/H^+ antiporter
EGF	Epidermal growth factor
EIPA	5-(N-ethyl-N-isopropyl) amiloride
EL	Extracellular loop
EMD 87580	N-(4,5-Bis-methansulfony-2-methyl-benzoyl) guanidine
ERM	Ezrin, radixin, and moesin
EtOH	Ethanol
Ex	Extracellular
G418	Geneticin
HA	Hemagluttinin
HEPES	N-2-hydroxyethylpiperazine-N'-2-ethanesulfonic acid
hNHE(#)	Human sodium proton exchanger isoform #
IL	Intracellular loop
In	Intracellular
IP	Immunoprecipitation
I/R	Ischemia/reperfusion

kb	Kilobase
kDa	Kilodalton
LB	Lysogeny broth
LF2000	Lipofectamine™ 2000 reagent
NCE	Na^+/Ca^{2+} exchanger
NHE	Na^+/H^+ exchanger
NHE1	Na^+/H^+ exchanger isoform 1
NHE(#)	Na^+/H^+ exchanger isoform (#)
NMR	Nuclear magnetic resonance
N-terminal	Amino terminal
PBS	Phosphate buffered saline
PCR	Polymerase chain reaction
pH_i	Intracellular pH
PIP_2	Phosphatidylinositol 4,5-bisphosphate
RSV	Rous sarcoma virus
RVI	Regulatory volume control
SDS-PAGE	Sodium dodecyl polyacrylamide gel electrophoresis
S.E.	Standard error
TBS	Tris-buffered saline
TE buffer	Tris and EDTA buffer
TM	Transmembrane
TM(#)	Transmembrane segments according to Landau's homology model
TM(Roman numerals)	Transmembrane segments according to Wakabayashi's topology
WT	Wild type

Chapter I

Introduction

1.1 Introduction, intracellular pH

Regulation of intracellular pH is tightly monitored by mechanisms that involve membrane compartmentalization and pH sensing proteins to prevent variations from the optimal pH ~7.2 (15). Minor alterations in intracellular pH can initiate allosteric reactions that affect the fate and function of cells in many ways. Proteins require specific pH ranges to fold correctly and their activity may be maximal within a narrow pH range (48). Additionally, proton gradients are essential for the generation of ATP in cellular respiration and to drive other passive ion transport proteins (22, 78).

Membranes and their associated ion transporters segregate and create the unique environments necessary for cellular functions (92). One of the main family of proteins that is responsible in maintaining intracellular pH is the Na^+/H^+ exchanger (NHE). Na^+/H^+ exchangers are membrane proteins that exchange H^+ for Na^+ across the lipid bilayer, thereby regulating pH, volume, and cation gradients in the cell (33). Na^+/H^+ exchangers are present in all kingdoms, and there are currently more than 200 NHE candidate genes (14).

1.2 Mammalian Na^+/H^+ exchangers

The mammalian Na^+/H^+ exchangers are ubiquitously expressed (33). Their activity and expression are vital to pH regulation, migration, growth, and development of cells (78). Nine human sodium proton exchanger isoforms have been characterized and a tenth isoform is still under investigation (70, 92). NHE isoforms perform electroneutral exchange of one intracellular H^+ for an

extracellular Na^+ (1:1 ratio), however each isoform has their own specific mode of regulation and cellular distributions (118). The isoforms share a similar membrane topology with 12 transmembrane helices and a C-terminal regulatory tail (41).

1.2.1 NHE1

The first isoform of mammalian NHE was identified in 1982 by Pouyssegur *et al.* (101). Pouyssegur's findings are still valid today, he established that i) NHE1 proton transport relies on Na^+ or Li^+, ii) the cation gradients provide the driving force and direction of exchange, iii) NHE1 is inhibited by amiloride and its analogues, and NHE1 is activated by growth factors (101). Since the first clone of NHE1 was isolated in 1989 by Sardet *et al.*, numerous studies on the function, kinetics, regulation, expression, structure and localization of NHE1 have been carried out in attempt to understand this important pH regulatory protein (113). NHE1 is composed of 815 amino acids which organize into two domains. The N-terminal transmembrane domain is responsible for cation translocation and the C-terminal regulatory domain in the cytoplasm regulates NHE1 activity (33). NHE1 is expressed in all tissues, including in the myocardium, and is localized to the plasma membrane and basolateral membrane of polar cells (32, 33). NHE1 is involved in several disease states such as hypertension, cardiac hypertrophy, myocardial ischemia and reperfusion injury, and cancer metastasis (78). NHE1 deficiency is tolerable in mice but NHE1-knockout mice developed ataxia, seizure, and growth retardation (10).

1.2.2 NHE2 - 10

Upon cloning and sequencing of the mammalian NHE1, additional isoforms have been identified by screening tissue libraries of different species using human NHE1 cDNA probes (92). NHE1 – NHE8 are highly homologous with the percentage identity ranging from 24 – 68% (33). hNHE2 has the highest sequence identity to hNHE1 at approximately 46% (92). NHE2 is expressed predominantly on the apical membrane of epithelial cells in colon and kidney, skeletal cells and to a lower level in testis, ovary, and small intestine (77, 79). Similar to NHE1, amiloride and 5'-amino alkyl substituted derivatives inhibit NHE2 cation translocation activity (77, 79). The function of NHE2 in rat cortical collecting duct cell line is to regulate steady-state intracellular pH and cell volume, whereas NHE1 activity is more responsive to intracellular acidosis (34). NHE2-null mice do not exhibit obvious disease phenotypes, however the parietal cells (stomach epithelial cells) show a net decrease in acid secretion compared to wild type during the infant stage, and various signs of degeneration in the adult phase (114). Therefore, the presence of NHE2 in parietal cells is essential for development and viability.

The amiloride insensitive hNHE3 contains 39% sequence identity to hNHE1 (13, 92). It is predominantly expressed on the apical membrane of the small intestine, colon, and kidney (41, 116). The primary role of NHE3 in the intestine and colon is to (re)absorb Na^+ and water into epithelial cells (3). In the kidney, NHE3 couples with Cl^-/base, formate or oxalate exchangers for the reabosorption of Na^+ and $NaHCO_3$ (5). The H^+ gradient created by NHE3 also

drives the uptake of other nutrients such as peptides and amino acids by other transporters (21, 126). Diarrhea, decreases in blood pressure, and acidic plasma pH were observed in NHE3-knockout mice (114).

NHE4 is highly expressed on the basolateral membrane of gastrointestinal tract cells and lower amounts are expressed in the kidney, brain, skeletal muscle, heart, uterus, and liver (12, 92, 100). NHE4 has properties distinct from NHE1, NHE2 and NHE3 isoforms. Expression of NHE4 in stably transfected fibroblast is activated by 4,4'-diisothiocyanostilbene-2,2'-disulfonic acid (DIDS) (16). Interestingly, DIDS is an anion exchanger inhibitor (51). The activity of NHE4 is highly resistant to treatment with amiloride and derivatives (13, 16). These results suggest that NHE4 is a highly specialized isoform of NHE. Knocking out NHE4 in mice gave effects similar to NHE2-null mice, with reductions in acid secretion, loss of parietal and mature chief cells and elevated amounts of undifferentiated, necrotic and apoptotic cells (35). Therefore, the function of NHE4 is for normal gastric secretion, cell growth and development (35).

NHE5's localization is predominantly in the plasma membrane and recycling endosomes of brain cells (8, 26). The shuttling of NHE5 between plasma membrane and recycling endosomes is mediated by secretory carrier membrane proteins (SCAMPs), which bind to NHE5 directly (26). NHE5 cation exchange activity is relatively insensitive to amiloride compounds and 5-(ethyl-N-isopropyl) amiloride inhibition similar to NHE3 (6, 124). NHE5 has been studied in end-stage renal disease and Familial Paroxysmal Kinesigenic Dyskinesia (121, 140).

NHE6 – 9 are found mostly or exclusively on the membranes of intracellular organelles (92). NHE6 and NHE9 are found in early and late endosomes respectively; NHE7 and NHE8 are distributed in trans-golgi network and mid-golgi network respectively (87). The function of NHE6 – 9 isoforms is to regulate the unique pHs of golgi bodies and endosomes (87). A loss of function mutation in NHE6 was found to be associated with the neurological disease angelman syndrome (110). The functional and physiological roles of NHE6 – 9 still remain to be further investigated.

NHE10 is expressed in osteoclasts in studies that attempted to identify proteins that contribute to osteoclastogenesis (70). Lee *et al.* isolated a putative sodium proton exchanger protein that had a transmembrane domain with 12 helices (70). However the sequence similarities of NHE10 to the known NHE1 – 9 are very low, approximately 12 – 14% (70). In addition, NHE10 does not seem to regulate pH_i; therefore more studies are required to determine if NHE10 is a true Na^+/H^+ exchanger (70).

1.3 Physiological roles of NHE1

NHE1 is an ubiquitous integral membrane protein composed of two distinct structural and functional domains. The N-terminal domain is responsible for Na^+/H^+ exchange and the C-terminal domain regulates the activity of NHE1 (118). NHE1 has several important physiological roles such as controlling cell pH as well as cell volume, cell proliferation and serving as a docking site and phosphorylation site for lipids and proteins (78). The latter functions of NHE1 are

implicated for cell migration and regulation of cation exchange activity. Dysfunctional NHE1 lead to pathologies such as hypertension, cardiac hypertrophy, ischaemia and reperfusion injury, and cancer metastasis (32).

1.3.1 NHE1 regulates intracellular pH and cell volume

In response to intracellular acidosis, NHE1 restores pH_i by exchanging one intracellular H^+ for one extracellular Na^+. The activity of NHE1 is stimulated by acidic pH, where at pH 6.5 NHE1 catalyzes at maximum activity (130). The activity of NHE1 is also dependent on cell volume. Cell shrinkage, induced under hypertonic or isotonic conditions, activates NHE1; This suggests that NHE1 responds to the change in cell volume instead of osmolarity (61). The increase in the intracellular Na^+ gradient, facilitated by the activity of NHE1, is coupled to the osmotic movement of water into the cell. This is also known as a regulatory volume increase which counteracts cell shrinkage (RVI) (23, 123).

It was observed that NHE1 hyperactivity and overexpression play contributing roles in hypertension, hypertrophy and ischaemia/reperfusion injury (32, 47). During cardiac ischemia-reperfusion, insufficient oxygen supply to cells induces anaerobic respiration; thus the production of lactic acid and protons from metabolism increase and this leads to intracellular acidification and activation of NHE1 (4, 99). As H^+'s get extruded, the intracellular concentration of Na^+ increases and this gradient provides the driving force for Na^+/Ca^{2+} exchanger. Elevated levels of intracellular Ca^{2+} initiate a cascade of cell events that cause cell injury, apoptosis, and necrosis (4, 7, 84). In many studies, hyperactivity and

overexpression of NHE1 have been suggested to contribute to cardiac hypertrophy and hypertension mediated through different pathways (29, 49, 52, 91, 93, 141). Studies inhibiting NHE1 activity or knocking out NHE1 have shown that the hypertrophic and hypertensive effects of NHE1 were attenuated (17, 29, 141).

1.3.2 NHE1 in cell differentiation and cell proliferation (cancer)

The expression level of NHE1 varies during cell differentiation and developments (65, 74, 108, 138). NHE1 activity is essential for mouse stem cell differentiation of cardiomyocytes. Inhibiting the activity of NHE1 rendered the development of normal cardiomyocyte. The amount of cell beating and the expression of cardiomyocyte specific protein α-MHC were depressed in EMD87580 (specific inhibitor of NHE1) treated embryoid bodies (74). In a mouse P19 embryonal carcinoma cell line, NHE-knockout reduced the rate of growth and propensity to differentiate into neuronal-like cells (134).

To study the role of NHE1 in cell growth, Pouyssegur and colleagues made an NHE deficient Chinese hamster lung fibroblast cell line (CCL39) by using a H^+-suicide technique (102). They found that the growth of NHE-deficient cells was highly reduced at neutral and acidic external pHs (pH<7.2). Whereas normal cells that expressed NHE were able to grow under a wide range of pH between 6.6 and 8.2 (102). These studies suggest that NHE is involved in regulating optimal pH_i for cell growth and differentiation.

One of the hallmark traits of cancer cells is an alkaline pH_i, which is suggested to be caused by the activity of NHE1 (38). Stimulated NHE1 activity is

observed widely in different types of transformed cells, and the inhibition of NHE1 ameliorates the development of cancer in some experimental studies (105-107). Interestingly, the NHE-deficient CCL39 cell line evolved into tumours at a slower rate compared to normal CCL39 after transformation and transplantation in mice (66).

1.3.3 NHE1 in cell migration and shape modeling (metastasis)

NHE1 is an integral protein that localizes to the front of migrating cells (37, 57). The C-terminal regulatory tail NHE1 contains a binding site for ERM (Ezrin/Radixin/Moesin), which links cytoskeletal protein actin filaments to NHE1 (25). The suggested roles of NHE1 are to anchor and organize the distribution of actin filaments to the plasma membrane (25). In addition, the activity of NHE1 is also essential for migration; an alkaline pHi is necessary for actin polymerization at the leading edge of migrating cells (122).

The activity of NHE1 generates an acidified extracellular micro environment to activate nearby matrix metalloproteases (MMPs) for the digestion of extracellular matrix. This facilitates the spread and migration of (cancerous) cells (53, 58). It is also proposed that the intracellular alkalinization contributed by NHE1 is able to elevate the expression of matrix metalloproteases (MMPs) and vascular endothelial growth factor (VEGF), which induce tumour growth and metastasis (40, 139).

Overall it is clear that the Na^+/H^+ exchanger isoform 1 is implicated in many pathologies. Elucidation of the mechanisms of transport and regulation will shed light on development of drugs for treating associated diseases.

1.4 NHE1 topology models

NHE1 is composed of 815 amino acids with an apparent molecular weight of 110kDa in the mature glycosylated protein (113, 115). There are two domains, the N-terminal domain consists of approximately 500 residues, which form the 12 transmembrane helices that span the plasma membrane and arrange into a porous structure for cation translocation; the C-terminal 315 residues of NHE1 form the cytoplasmic regulatory tail that contains binding sites for lipid, proteins, and sites of phosphorylation by kinases (113, 132).

1.4.1 Wakabayashi *et al.* model of NHE1

Two topologies are currently proposed for NHE1. In the year 2000, Wakabayashi *et al.* determined a detailed NHE1 membrane topology by substituted cysteine accessibility analysis (132). Cysteine mutations were introduced in selected residues that were thought to be located on either the extracellular or intracellular loops, based on the predicted Kyte-Doolittle algorithm hydropathy analysis model (62). Then the cysteine mutants were treated with MTSET and biotin-maleimide under normal and membrane permeabilized conditions. Cysteine residues that were labelled with biotin-maleimide under normal conditions were considered as extracellular, however

when they were treated with MTSET prior to biotin-maleimide labelling, MTSET was able to modify the accessible cysteines and block any further labelling. Intracellular residues were only exposed to MTSET and biotin-maleimide under permeablized conditions (132). By locating the MTSET accessible residues on the membrane surface and then by locating the restricted residues intracellularly, the orientation and configuration of NHE1 transmembrane segments were resolved. Wakabayashi *et al.*'s NHE1 topology (Figure 1) presents a model with 12 transmembrane helices (average of 21 – 22 amino acids per segment), short intracellular N-term head and a long C-term tail, large extracellular loop 1, and three re-entrant loops.

1.4.2 Topology model of NHE1 with EcNhaA

A new topology of NHE1 was suggested by Landau *et al.* in year 2007, shortly after publication of the *E. coli* Na^+/H^+ antiporter (EcNhaA) crystal structure (45, 67) (Figure 1). Landau *et al.* constructed a 3D-model of NHE1 using sequence alignment and the EcNhaA crystal structure as a template. Although the sequence similarity of NHE1 and EcNhaA is approximately 10%, Landau *et al.* affirmed that the predicted structure of NHE1 is validated empirically and backed up by evolutionary conservation analysis (67). The topology of the 3D-model of NHE1 also contained 12 transmembrane helices with a large C-terminal tail starting past amino acid number 505. Yet, this topology does not have any re-entrant loops that are found in the Wakabayashi's model. (Figure 1) TM1 in Landau's topology model begins at Val129, whereas TMI in

Wakabayashi's model starts at His13. Landau suggested that the first two transmembrane helices of NHE1 are cleaved as signal peptides. Topogenesis studies on NHE1, NHE3, and NHE6 indicated that these isoforms contain a signal peptide in their first hydrophobic segments (80, 142). Moreover, NHE2, NHE4, and NHE5 are predicted to contain signal peptides by the program SignalP tools (89, 90). In addition, it has been demonstrated that removal of the first two transmembrane helices (the first 150 N-term amino acids) of NHE1 does not render cation exchange activity (115). Contrary to the suggestions that TMI and TMII are redundant, the existence of N-linked glycosylation on extracellular loop 1 is highly recognized and detected in the mature form of NHE1 (20, 39). Another feature of the new model is that TM7 (331 – 344) and TM8 (349 – 362) are only 14 residues long, which is much shorter than the average length of TM segments with 21 – 22 residues.

1.5 Structure of NHE1

Even though obtaining the high resolution crystal structure of NHE1 is still an ongoing project, several attempts using homology model analysis, biochemical techniques, NMR spectroscopy, electron microscopy, and circular dichroism spectroscopy have been able to reveal significant insights on the secondary and tertiary structure of NHE1 (67, 82, 104).

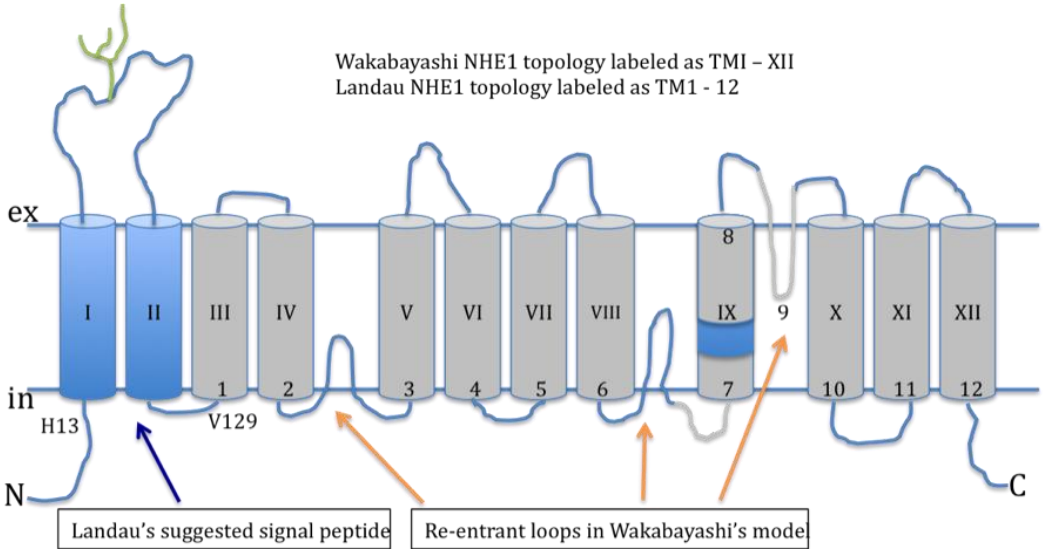

Figure 1. NHE1 membrane topology models. The two models of NHE1 topology are illustrated. The Wakabayashi *et al.* model is indicated by the roman numerals (I-XII), and TM segments are colored in blue and gray. While the Landau *et al.* model is numbered 1-12 and is in gray only (67, 132). TMI and II are cleaved as signal peptide in Landau's model. Three re-entrant loops in Wakbayashi's model are labelled. The two short TM7 and TM8 segments in Landau's model are part of the TMIX in Wakabayashi's topology. TM9 from Landau's model spans the re-entrant loop position of Wakayashi's model. ex:extracelluar, in:intracellular.

1.5.1 Dimeric structure of NHE1

NHE1 forms a homodimer in the plasma membrane with a few direct intermolecular contacts on the cytoplasmic tail. Using sulfhydryl reactive crosslinkers such as Cu^{2+}/o-phenanthroline, disuccinimidyl suberate, or bifunctional methane thiosulfonate, stable dimers and monomers of NHE1 were resolved on SDS-PAGE with a molecular weight of approximately 210 kDa and 110 kDa respectively (30, 43, 44). Evidence suggested that the 562 – 579 amino acids region of the NHE1 is responsible for dimerization, deletion of this region abolishes intermolecular interaction (30). Further investigation demonstrated that the intrinsic cysteines Cys794 and Cys561 on the cytoplasmic regulatory tail contribute to dimer formation (44).

1.5.2 Structural analysis of purified full length NHE1

For electron microscopy imaging of NHE1, the purified protein was mounted onto a carbon-coated grid and a series of images were examined under a microscope to produce a structure of NHE1 at 22 Å resolution (82). The full length (1 – 815aa) NHE1 was a homodimer in proteoliposomes with a dimension of 100 Å x 100 Å x 90 Å (82). In this study, the molecular weight was verified by size-exclusion chromatography and it corresponded to ~220 kDa, the weight of an NHE1 homodimer. Extensive contacts in the cytoplasmic domains were found in NHE1 homodimer suggest that this region contributes to intermolecular contact and stabilization (82). The secondary structure profile of NHE1 was determined

by circular dichroism spectroscopy. This indicated that the overall framework of NHE1 is composed of 41% α-helix, 23% β-sheet, and 36% random coil (82).

1.5.3 Structural determination of transmembrane segments of NHE1 by NMR spectroscopy

In addition to X-ray crystallography, NMR spectroscopy is another useful method for determining the atomic level structure of small proteins or peptides that have molecular weights below 20 kDa (136). Four isolated transmembrane segments according to the Wakabayashi topology, TMIV, TMVII, TMIX, and TMXI of NHE1 have had their structure determined using NMR spectroscopy (28, 69, 104, 120, 132). A peptide of TMIV produced in *E. coli* (155 – 180aa) was examined in CD_3OH:$CDCl_3$:H20 and did not exhibit a uniform α-helical structure found in some canonical transmembrane helices (118). TMIV was comprised of coil (159 – 163 aa), an extended segment (165 – 168 aa), β-turn (174 – 175 aa) , and a very short α-helical region (169-176 aa). A synthetic peptide of TMVII (251 – 273 aa) was examined in dodecylphosphocholine (DPC) micelles (28). The structure of TMVII is primarily α-helical, with a break in the centre of this peptide between Gly261 and Glu262. The N- and C-terminal regions were also slightly extended (28). Glycine is known to disrupt continuous helices due to its flexible backbone rotation and Gly261 was found in the extended region of the segment (50). The NMR structure of a synthetic peptide of TMIX (339 – 363 aa) in DPC micelles had a L-shaped conformation, with N- and C- terminal helix regions (340 – 344 aa and 353 – 359 aa) connected by a large kink at Ser351,

which bent the peptide to approximately 90^{o} angle (103). NMR structural analysis on a synthetic peptide of TMXI (449 – 470 aa) in DPC micelles indicated that this segment represents a discontinuous helix (69). N- and C-terminal regions (447 – 454 aa and 460 – 471 aa) were helical, in between there was an unstructured loop that spanned from 455 – 459 aa, which contained two glycine residues (69).

1.5.4 Crystal structure of the *Escherichia coli* sodium proton antiporter

The crystal structure of the *E. Coli* Na^{+}/H^{+} antiporter (EcNhaA) was solved at a resolution of 3.45 Å (45). EcNhaA and NHE1 are distantly related with a sequence identity of only ~10%. They belong to the same cation/proton antiporter superfamily and exchange H^{+} for Na^{+} across the membrane bilayer (14). However the stoichiometry of EcNhaA Na^{+}/H^{+} exchange is $1Na^{+}:2H^{+}$. In addition, EcNhaA is activated by alkaline instead of acidic pH and it translocates cations in the opposite direction compared with NHE1 (45, 135). EcNhaA activity allows prokaryotes to survive in an environment containing external sodium (60, 92). The 388 amino acid residues of NhaA is roughly half of that of NHE1 (45). The crystal structure of EcNhaA showed 12 transmembrane segments that arrange into a conformation with two funnels that have wide openings facing the cytoplasmic and periplasmic sides (45). The centre of EcNhaA narrowed, preventing the formation of a continuous pore; this was likely because the protein was crystallized in an inactive conformation. The funnels are constructed primarily by two discontinuous helices TM4 and TM11; they cross

over each other at their extended regions in anti-parallel orientation (45). Between the positive helix dipoles of TM4 and TM11 lies a negatively charged Asp133 that compensates for the like-charge repulsion, and a positively charged Lys300 is positioned halfway between the negative helix dipoles (45). The proposed residues coordinating cations are Asp163 and Asp164 on TM5, which is in close proximity to the TM4/11 assembly (45).

1.5.5 Constructing NHE1 structure by homology modeling with EcNhaA

A 3D-model structure of NHE1 based on the crystal structure of EcNhaA was constructed by Landau *et al.* (67). The methods for NHE1 structure development included evolutionary conservation analysis along with the application of the homology modeling program NEST (67, 98). The N-terminal transmembrane domain of the NHE1 homology model is composed of 12 transmembrane helices (129 – 507 aa) with an orientation and overall structure similar to EcNhaA (67). Evolutionary conserved residues are mostly found in the core of NHE1, whereas the variable residues are located on the protein surface (67). The disrupted helices of TM4/11 assembly are also presented in this NHE1 model, their helix dipoles are compensated for by a negatively charged Asp238 in TM4, and a positive Arg425 in TM10 (67). Asp267 in TM5 corresponds to the titrating residues of Asp163 – Asp164 of EcNhaA. The pore is formed by transmembrane helices 2, 4, 5, 8, and 11; they are proposed to be either pH sensing or controlling cation translocation across the membrane by opening and closing of the funnels (67).

1.6 NHE1 Na^+/H^+ exchange mechanism

NHE1 is classified as a secondary active transporter, the driving force for its activity is prompt by the Na^+ and H^+ concentration gradients, ATP is not directly required although it may modify NHE1 activity through an ancillary factor (1). The activity of NHE1 strictly requires Na^+ and H^+, however NHE1 is also capable of translocating extracellular Li^+ for intracellular H^+ (55, 92). Interestingly, the direction of cation exchange is reversible, and dependent on the cation gradients imposed upon the membrane (101).

1.6.1 NHE1 kinetics

NHE1 is quiescent at physiological pH_i of ~7.2, and activates during acidosis (33). Kinetics of NHE1 cation transport are suggested to obey the Monod-Wyman-Changeux model, such that the presence of protons and intracellular activating signals induce molecular transitions in NHE1 (15, 63, 83). NHE1 exists as a homodimer on the plasma membrane, and their affinities to intracellular protons shift in equilibrium between high and low states (63, 82). The inactive low affinity state is favoured by an equilibrium during physiological pH; however at acidic pH, the equilibrium shifts towards the active proton-stabilized high affinity state (63, 64). The results of analysis of NHE1 kinetics proposed the presence of two protonation sites, and cooperative regulation of a dimeric NHE1 protein (63). Dimerization of NHE1 is essential for cation transport. Truncations of C-terminal regions diminished dimerization and cation exchange by approximately 10-fold (44).

1.6.2 Cation exchange mechanism of EcNhaA and NHE1

According to the crystal structure of EcNhaA, the mechanism of cation exchange activity relies mainly on the TM4/11 assembly, the Asp163-Asp164 cation binding residues, and the pH sensor TM9 (45). Upon intracellular alkalinization, TM9 responds to pH change by a conformational shift, which then induces the opening of the intracellular facing funnel formed by TM4/11 (45). The Na^+ binding site is now accessible at Asp163-Asp164 on TMV. Binding of positively charged Na^+ to the cytoplasmic funnel causes a charge imbalance and initiates a movement in the flexible loops of the TM4/11 assembly (45). A series of conformational changes closes the cytoplasmic funnel and opens up the periplasmic funnel thereby releasing Na^+. Two protons then immediately bind to Asp163 and Asp164 from the periplasm, and trigger another conformational shift of the TM4/11 assembly which opens up the cytoplasmic funnel (45). Deprotonation of Asp163-Asp164 releases two protons into the cytoplasm and reverts the antiporter back to its resting state, ready for next round of transport (45). A similar mechanism of cation translocation is proposed by Landau *et al*. based on the homology model structure of NHE1 (Figure 2) (67). The TM4/11 assembly is essentially directing the movement of cations by exercising the opening and closing of funnels. Intracellular acidosis introduces conformational change in NHE1, which opens up the cytoplasmic funnel and allows Asp267 protonation (67). The binding of a proton to Asp267 triggers the opening of extracellular funnel. Once the proton dislocates from Asp267 a sodium ion

interacts electrostatically with Asp267, and again causes a conformational change in the TM4/11 assembly which transfers the sodium to the intracellular side (67).

1.6.3 Functionally important residues of NHE1

In order to characterize the function of NHE1, many amino acids and segments were investigated by mutation and truncation analysis. These studies examined cation translocation, pH sensing, dimerization, and surface localization. Residues that make up the cation translocation pore of NHE1 were identified by cysteine scanning mutagenesis and reaction with sulfhydryl reactive compounds: Phe161 in TMIV; Leu255 and Leu258 in TMVII; Glu346 and Ser351 in TMIX; Leu457, Ile461, and Leu465 in TMXI are pore lining residues (transmembrane segments are assigned according to Wakabayashi topology model) (28, 69, 103, 120).

Several residues (Phe161 – Leu163, Ile169, Ile170, and Gly174) in TMIV are suggested important for the binding of inhibitor amiloride and cariporide; mutational analysis on these amino acids have greatly reduced NHE1 sensitivity to inhibitors (18, 19, 56, 127). Asp267 is thought to be the putative protonation site in the cation translocation pore of NHE1, substituting Asp267 to Ala and Cys exhibited profound decreases in transport activity (27, 28). pH sensing regions on NHE1 are proposed to be in the 516 – 590 amino acids region, deleting this segment removed the pH_i sensitivity in the absence of ATP (46). Other putative pH sensing amino acids are Arg440, Gly455, and Gly456 in intracellular loop V; substituting Arg440 to Cys, His, Asp, Leu, and Glu shifted the NHE1 pHi

dependence to the acidic side, whereas mutation of Gly455 to bulky amino acids caused an alkaline shift (131).

Internalization of NHE1 mutants is commonly observed. Leu156Cys, Asp159Cys, Pro167Cys, Pro168Cys, Asp172Cys, Gly309Val, Ile451Cys, Tyr454Cys, Gly455Cys, Gly456Cys, Arg458Cys, and Gly459Cys mutations were retained intracellularly as the immature form of NHE1. In addition, internalized NHE1 mutants were incapable of rectifying acidified pH_i (43, 69, 119). Interestingly, looking at the localization of Tyr454Cys and Arg458Cys mutants under immunofluoresence microscopy revealed their retention in the endoplasmic reticulum (133).

1.7 NHE1 regulatory mechanisms

The study on NHE1 regulation pathways is very complicated due to a large number of associated factors, but it is crucial to understand the mechanisms underlying the regulation of NHE1 in order to develop drugs that are beneficial for treating cancer and cardiac diseases. Amiloride is a low potency inhibitor of NHE1 and its modification to EIPA improves its potency and specificity. The inhibitors cariporide HOE642 and HOE694 are benzoylguanidines and are more selective and potent inhibitors (97). Cariporide had been administered to patients in clinical trials for the treatment of cardiac ischemia and reperfusion injury, however the outcomes in separate studies were contradictory and no significant improvement was observed except in some subgroups (111, 125). The N-terminal

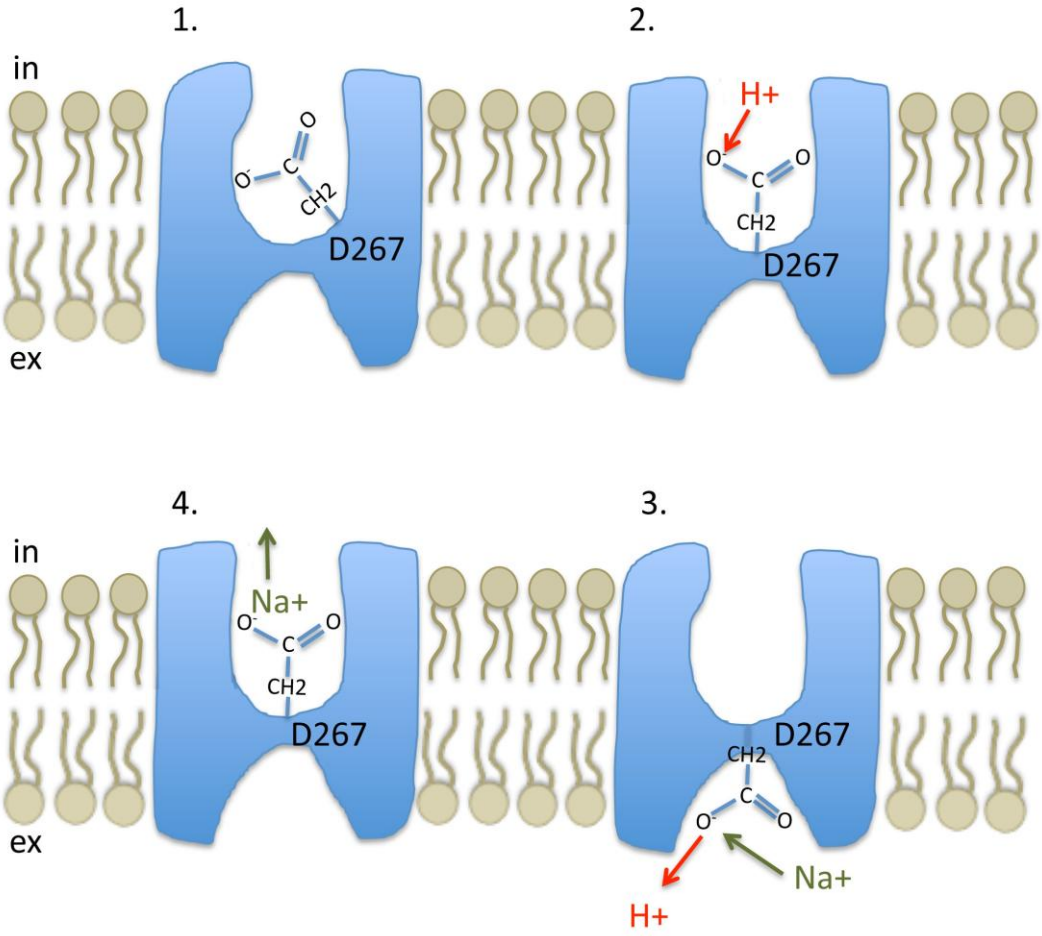

Figure 2. Landau *et al.* proposed Na^+/H^+ exchange mechanism for NHE1 (67). This model represents the activity mechanism of NHE1 with its putative cation binding residue Asp267. 1) NHE1 resting state contains a closed intracellular funnel with an inaccessible deprotonated Asp267. 2) Increases in intracellular H^+ activates NHE1 by inducing conformational changes that opens up intracellular funnel, thereby allowing H^+ association with Asp267. 3) Binding of H^+ to Asp267 causes a charge imbalance that reorients Asp267 to the extracellular funnel. Deprotonation of Asp267 is followed by the uptake of extracellular Na^+. 4) Association of Na^+ in translocation pore induces another conformal change that opens up the intracellular funnel and releases Na^+. NHE1 goes back to the resting state and prepares for another round of Na^+/H^+ exchange (67).

transmembrane domain of NHE1 contains inhibitor binding regions for amiloride derivatives and cariporide. TMIV and TMIX may contain part of the inhibitor binding site (97). Mutations in Phe165 and Leu167 of TMIV, Glu350 and Gly356 of TMIX have abolished inhibitor sensitivity (18, 56). Epidermal growth factor (EGF), thrombin, serum, insulin, and lysophosphatidic acid (LPA) and angiotensin-II are stimulatory regulators of NHE1 (68, 92, 101, 112, 129).

The activity of NHE1 is tightly regulated by signalling molecules, hormones, secondary messengers, kinases, lipids and adaptor proteins, (78). The 315 amino acid C-terminal regulatory tail of NHE1 contains numerous binding sites for molecular interaction and modification. The association of phosphatidylinositol 4,5-bisphosphate (PIP_2) to NHE1 is essential for optimal activity and is related to intracellular ATP concentrations. Depletion of ATP decreased the cation exchange activity and the binding of PIP_2 to NHE1 (2). Removal of PIP_2 putative binding sites on C-terminal tail of NHE1 also decreased ion transport (2). Calcinuerin homologous protein 1 (CHP1) binds to amino acids 510-530 of the NHE1 tail in a Ca^{2+} dependent manner, and the association is necessary for normal cation exchange activity (94-96). ERM proteins are bound to amino acids 533-564 of NHE1 and they link actin filaments near the plasma membrane and aid in cell migration and maintenance of cell structure (24, 25). Calmodulin (CaM) is another Ca^{2+} sensitive secondary messenger that binds to two sites on NHE1: it binds to a high affinity site at amino acids 636 – 656 and to a low affinity site at amino acids 657 – 700 (11). The contribution of CaM in NHE1 function is to remove the effects of an autoinhibitory domain when Ca^{2+}

levels are high. It does this by binding to the high affinity CaM site (11). The binding of 14-3-3 to phosphorylated Ser703 is stimulated by serum, and may represent a downstream candidate pathway for serum activation of NHE1 cation translocation (71). Tescalcin was shown to bind to the C-terminal tail of NHE1 in a Ca^{2+}-dependent manner. Its association has inhibitory effects on NHE1 activity (73, 76). An enzyme that catalyzes the formation of HCO_3^- and H^+ from CO_2 is carbonic anhydrase II (CAII). It interacts directly with NHE1 C-terminal tail around amino acids 790 – 802 (75). The H^+ produced by CAII can be quickly exported by its nearby binding partner NHE1. Therefore the direct binding interaction between CAII and NHE1 enhances the extrusion of H^+ (72).

1.8 Thesis objective

Our laboratory has previously investigated the functional and structural properties of the important NHE1 transmembrane segments IV, VII, IX, and XI, as assigned in the Wakabayashi's topology model (28, 69, 103, 120, 132). These studies yielded significant insights into the understanding of the mechanism of NHE1 transport. TMVI in Wakabayshi's model is equivalent to TM4 in Landau's homology model of NHE1 (67). The EcNhaA crystal structure and the NHE1 homology model suggest that a TM4/11 assembly forms a key part of two flexible funnels that are involved in cation translocation. The TMVI segment of Wakabayashi model (227 – 249 aa) has never been thoroughly studied and its functional contribution to NHE1 activity is not well characterized. According to the homology structure, amino acids 226 – 248 are important in the formation of a

cation translocation pore and facilitation of cation exchange. In this work, cysteine scanning mutagenesis was applied to investigate TMVI amino acid residues 227 – 249. By treating each TMVI cysteine mutant with sulfhydryl reactive reagents and monitoring for inhibition of NHE1 activity, we were able to identify residues lining the cation translocation pore and involve in cation exchange. Further studies examined the specific requirements for amino acids at critical locations and the nature of the defects present at amino acids important in transport.

Chapter II

Materials and methods

A version of this chapter on NHE1 TMVI cysteine mutations also appears in the Journal of Biological Chemistry (2010) 285:36656-65. Jennifer Tzeng, Brian Lee, Brian Sykes and Larry Fliegel.

2.1 Oligonucleotides for TMVI mutagenesis

The program DNA strider 1.4 was used to design the oligonudcleotides used for mutation of NHE1. For cysteine scanning mutagenesis, each residue of TMVI from Asn227 to Ile249 was mutated into a cysteine and a new silent restriction enzyme site was introduced for screeening purposes. We used the plasmid pYN4+c as template (Figure 3), which encoded for the entire cysteineless NHE1 (cNHE1) with a hemmaglutinnin (HA) tag at the C-terminal end. The original 10 native cysteines in NHE1 were mutated into serines in this plasmid. Previous studies on the expressed cNHE1 showed that the activity and surface localization were not significantly different from the wild type NHE1 (119).

Residues in TMVI that were critical to activity or that were inhibited by MTSET were mutated into other amino acids (i.e. Asn227Ala, Asn227Asp, Asn227Arg, Ile233Ala, Leu243Ala, Glu247Asp, Glu247Gln, Glu248Asp, and Glu248Gln) in the pYN4+ wild type NHE1 plasmid template. Again, new silent restriction enzyme sites were introduced (Table 1).

Mutation	Oligonucleotide Sequence	Restriction Site
	pYN4+ Cysteineless Plasmid	
N227C	5’-CAACAACATCGGCCT**tCTaGA**CtgCCTGCTCTTCGGCAGC-3’	*Xba I*
L228C	5’-CGGCCTCCTGGA**CAAttg**cCTCTTCGGCAGCATC-3’	*Mfe I*
L229C	5’-CTCCTGGACAACCTGtgCTTCGG**atcgAT**CATCTCGGCCGTG-3’	*Cla I*
F230C	5’- CTGGACAACCTGCTCTgC**GGatcC**ATCATCTCGGCCGTG -3’	*Bam HI*
G231C	5’-GACAACCTGCTCTTCtGCAGCATCATCT**CcGCgG**TGGACCCCGTG GCG-3’	*Sac II*
S232C	5’-CAACCTGCTCTTCGG**atGCAT**CATCTCGGCCGTG-3’	*Nsi I*
I233C	5’-CTGCTCTTCGG**CAGCtg**CATCTCGGCCGTGGAC-3’	*Pvu II*
I234C	5’-GCTCTTCGGCAG**CATatg**CTCGGCCGTGGACCC-3’	*Nde I*
S235C	5’-CTTCGGCAGCAT**CATaTg**cGCCGTGGACCCCGTG-3’	*Nde I*
A236C	5’-GGCAGCATCATCTCGtgC**GTcGAC**CCCGTGGCGG-3’	*Sal I*
V237C	5’-CAGCATCATCTCG**GCatgc**GACCCCGTGGCGG-3’	*Sph I*
D238C	5’-CGGCAGCATCATCT**CcGCgG**TGtgCCCCGTGGCGGTTC-3’	*Sac II*
P239C	5’-CATCATCTCGGCC**GTcGAC**tgCGTGGCGGTTCTGG-3’	*Sal I*
V240C	5’-TCGGCCGTGGACCCC**tgcGCa**GTTCTGGCTGTCTTTG-3’	*Fsp I*
A241C	5’-GCCGTGGACCCCGTGtgcGT**gCTaGC**TGTCTTTGAGG-3’	*Nhe I*
V242C	5’-CGTGGACCCCGTG**GCatgc**CTGGCTGTCTTTGAG-3’	*Sph I*
L243C	5’-GACCCCGTGGCGGTT**tgcGCa**GTCTTTGAGGAAATTC-3’	*Fsp I*
A244C	5’-CGTGGACCCCGTGGC**aGTaCT**GtgTGTCTTTGAGGAAATTC-3’	*Sca I*
V245C	5’-CGTGGCGGTTCTG**GCatgC**TTTGAGGAAATTC-3’	*Sph I*
F246C	5’-GCGGTTCTGGCTGTCTgTGAGGA**gATTCACATC**AATGAG-3’	*Bsa BI*
E247C	5’-GTTCTGGCTGTCTTTtgcG**AgATTCACATC**AATGAG-3’	*Bsa BI*
E248C	5’-TCTGGCTGTCTTTGA**atgcAT**TCACATCAATGAG-3’	*Nsi I*
I249C	5’-GCTGTCTTTGAG**GAAtgcC**ACATCAATGAGCTG-3’	*Bsm I*
	pYN4+ WT NHE1 Plasmid	
N227A	5’-CAACAACATCGGCCT**tCTaGA**CgcCTGCTCTTCGGCAGC-3’	*Xba I*
N227D	5’-CAACAACATCGGCCT**tCTaGA**CgACCTGCTCTTCGGCAGC-3’	*Xba I*
N227R	5’-CAACAACATCGGCCT**tCTaGA**CcgCCTGCTCTTCGGCAGC-3’	*Xba I*
I233A	5’-CTGCTCTTC**GGatcC**gcCATCTCGGCCGTGGAC-3’	*Bam HI*
L243A	5’-GACCCCGTGGCGGTTg**ccGCgG**TCTTTGAGGAAATT-3’	*Sac II*
E247D	5’-GTTCTGGCTGTCTTTGAcGA**gAT**TCAC**ATC**AATGAG-3’	*Bsa BI*
E247Q	5’-GTTCTGGCTGTCTTTcAGGA**gAT**TCAC**ATC**AATGAG-3’	*Bsa BI*
E248D	5’-TCTGGCTGTC**TTcGAa**GAcATTCACATCAATGAG-3’	*Bst BI*
E248Q	5’-TCTGGCTGTC**TTcGAacAA**ATTCACATCAATGAG-3’	*Bst BI*

Table 1. Synthetic oligonucleotide primers for site directed mutagenesis of NHE1 TMVI. All primers contain a point mutation (lower case) and a new restriction site (bold). TMVI cysteine mutant primers were designed using a pYN4+ cysteineless plasmid as template. Other TMVI mutations were introduced into the wild type pYN4+ plasmid (containing the normal cysteines of NHE1).

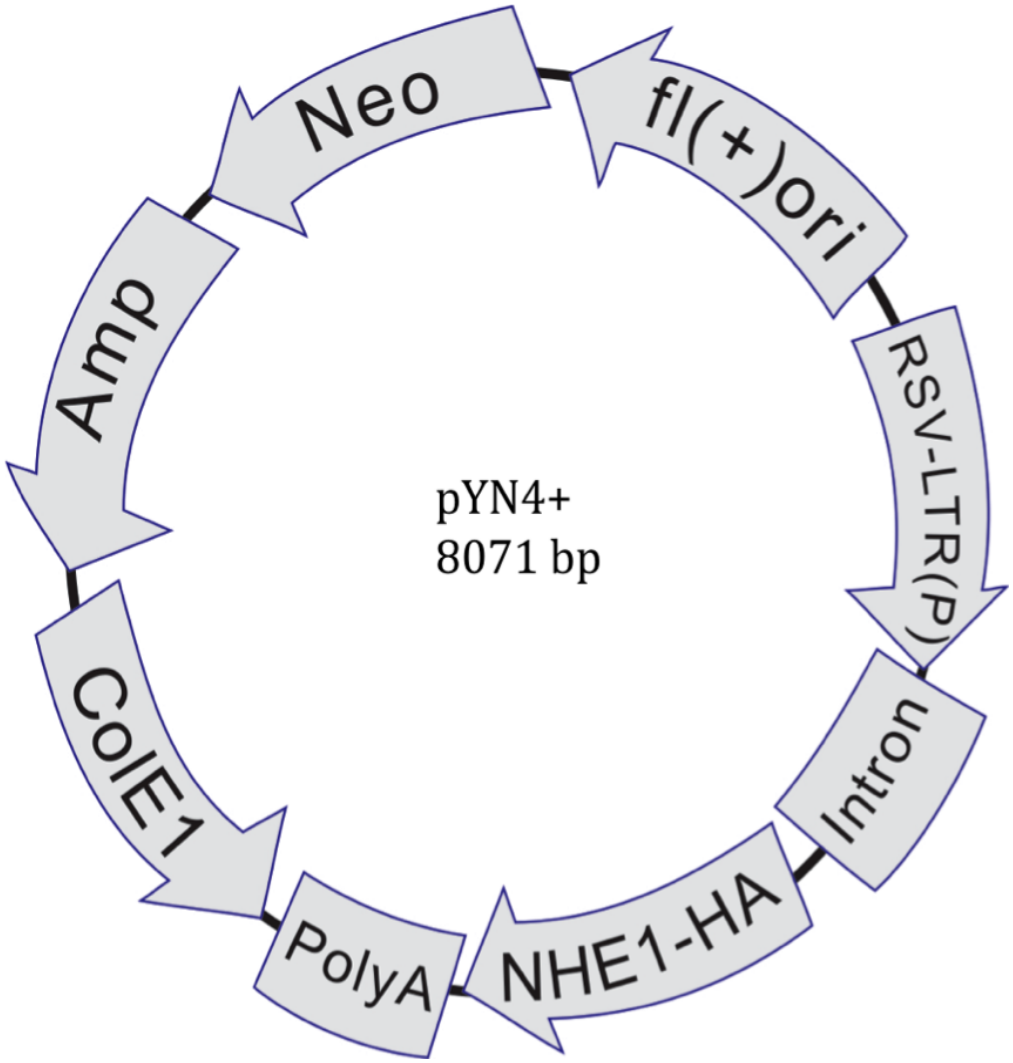

Figure 3. Circular map of pYN4+ plasmid. Primer design and site-directed mutagenesis were carried out using pYN4+ plasmid. NHE1 with a C-terminal HA-tagged gene was inserted from bp 3066 to 5666. The 8071bp plasmid is composed of a Rous Sarcoma Virus long terminal repeat promoter (RSV-LTR(P)), Amp resistance gene, f1(+) ori (phage replication origin), ColE1 (bacterial replication origin), Neo (neomycin resistance cassette), PolyA (polyadenylation tail), and intron (upstream promoter and enhancer region of NHE1). The Neo gene is required for stable cell line selection by G418 antibiotic during transfection.

2.2 Polymerase Chain Reaction (PCR) for site directed mutagenesis

Site directed mutagenesis for NHE1 TMVI was performed using polymerase chain reaction (PCR). The pYN4+ cNHE1 plasmid was denatured at 60^{o}C for 15 minutes prior to addition of PCR reaction solutions. All preparatory steps were carried out on ice. Two sample mixtures were prepared in eppendorf tubes labelled as A and B. PCR sample mixture A contained 5 μl of 2.5 mM dNTP mix (dATP, dTTP, dCTP, dGTP), 9 μl of ddH_2O, 1 μl of plasmid template at 0.75 μg/μl, 5 μl of 10 μM forward primer and 5 μl of 10 μM reverse primers. Sample mixture B contained 19.5 μl ddH_2O, 5μl PWO buffer + MgSO4, and 0.5 μl PWO polymerase. Samples A and B were mixed immediately prior to incubation in the Techne Thermal Cycler TC-312. The PCR consisted of 18 cycles. Each cycle included a denaturing step at 95^{o}C for 30 sec, annealing step at 55^{o}C for 1 min, and an elongation step at 68^{o}C for 20 min. PWO DNA polymerase was obtained from Roche Applied Science (Roche Molecular Biochemicals, Mannhein, Germany).

2.3 *E. Coli* transformation

The products from PCR were digested with the enzyme DpnI for 4 - 5 hours at 37 ^{o}C. DpnI was purchased from Invitrogen (Carlsbad, CA, USA). 1 – 3 μl of the digested plasmid was transformed via electroporation into electrocompetent *E. Coli* DH5α. Cells were left to recover in 500μl lysogeny broth (LB) medium at 37^{o}C for 1 hour. *E. coli* were then plated on 0.15μg/L ampicillin (Amp) LB agar plates, and allowed to grow overnight in 37^{o}C incubator.

2.4 Plasmid isolation from *E. coli*

Single *E. coli* colonies were picked from LB ampicillin plates the day after transformation and were cultured overnight in 1.5 ml LB at 37^{o}C with agitation. Plasmids were isolated by following established laboratory DNA extraction protocols. Cells were collected by centrifugation at 10000 rpm for 3 min. Cell pellets were re-suspended in 150 μl P1 buffer (50 mM Tris pH8.0, 10 mM EDTA, 100 μg/ml RNase) and left at room temperature for 10 min. 150 μl of P2 lysis buffer (200 nM NaOH, 1% SDS) was added into the mixture and mixed thoroughly until the lysate turned viscous. 150 μl of cold P3 neutralization buffer (3MKCH_3COO^-, 1.5% glacial acetic acid) was then added, mixed briefly and left on ice for 10 min. The white fluffy precipitates formed contained genomic DNA, proteins, and cell debris; they were removed by centrifugation at 14000 rpm for 5 min. The supernatant was transferred to a new eppendorf tube, and 150 μl of phenol-chloroform (25 phenol: 24 chloroform: 1 isoamyl alcohol) was added to extract plasmid DNA. The mixture was vortexed briefly and centrifuged at 14000 rpm for 5 min. The top aqueous layer of the two layered heterogeneous liquid was transferred into a new eppendorf tube. The plasmid DNA was then precipitated in 1ml cold 100% EtOH at -20^{o}C for at least 20 min, and centrifugation at 14000rpm for 5 min. The DNA pellet was washed with 70% EtOH and dissolved in 60 μl of ddH_20.

2.5 Restriction digestion and agarose gel electrophoresis

Mutant plasmids containing putative new restriction sites were digested with appropriate enzymes to check for the introduced mutations. The reaction mixture was composed of 5 μl plasmid, 1 μl of restriction enzyme, 0.5μl of 1mg/ml RNase, 0.2 μl BSA (if required), 2 μl of 10X reaction buffer and ddH_20 was added to a total of 20 μl. Most of the digestion reactions were carried out at 37°C incubator for 2 hours. In some cases, the restriction enzymes required 25°C, 60°C or 65°C for optimal activity and were therefore carried out at these temperatures. Restriction enzymes were purchased from New England Biolabs (Ontario, Canada) and Invitrogen. Plasmids digested with restriction enzymes were separated on 1% agarose gels containing 0.5 mg/ml ethidium bromide. 6X DNA loading buffer was added in order to track the migration progress. A 1kb plus DNA ladder was used to estimate plasmid fragment size. The agarose gel was visualized under UV light and gel pictures were taken with a video copy processor. DNA fragment band patterns were used to select for positive mutants.

2.6 Large scale DNA preparation

Large scale plasmid purification from *E. coli* was achieved by using QIAGEN plasmid maxi kits and following their protocol. Colonies that expressed plasmids with positive mutations were cultured overnight in 150 ml LB containing 150 μl of 100 mg/ml ampicillin. The cells were then harvested by centrifugation at 6000 g for 15 min at 4°C. Pellets were re-suspended in cold 10 ml P1 buffer (50mM TrisCl pH8.0, 10mM EDTA, 100μg/ml RNase A, 1μl LyseBlue/P1 ml). 10 ml P2

(200mM NaOH, 1% SDS (w/v)) was added immediately and then mixed gently until the lysates turned blue (an indication of well-mixed solution). The mixture was then allowed to sit no more than 5 min at room temperature. 10 ml ice cold P3 (3 M potassium acetate pH5.0) was added and the mixture was incubated on ice for 20 min. Centrifugation was at 20000 g for 30 min at 4^{o}C and removed most of the precipitates (containing genome DNA, proteins, and cell debris) that formed in the mixture. A second centrifugation at 20000 g for 15 min at 4^{o}C removed remaining precipitates. The supernatant was loaded in an equilibrated QIAGEN-tip 500 to allow binding of plasmid DNA to the column. The column was washed twice with 30 ml QC buffer (1.0 NaCl, 50 mM MOPS pH7.0, 15% isopropanol (v/v)) and eluted with 15 ml QF buffer (1.25 NaCl, 50 mM TrisCl pH8.5, 15% isopropanol (v/v)). Plasmid DNA was precipitated with 10.5 ml isopropanol and centrifuged at 15000 g for 30 min at 4^{o}C. DNA pellets were washed with 70% EtOH and allowed to air dry. 400 μl of TE buffer (10 mM Tris, 1 mM EDTA) was added to re-dissolve plasmid.

2.7 DNA Sequencing

Plasmids acquired from QIAGEN Maxi-kit were sequenced to confirm mutation sites. 260 nM concentration of plasmid DNA and a 2 pmol/μl of primer approximately 100 bp upstream of mutation site were used for sequencing. All DNA sequences were performed at the University of Alberta, Department of Biochemistry, DNA Core Services Laboratory.

2.8 Transfection of AP-1 cells and stable cell line generation

WT, cNHE1, and mutant plasmids were stably transfected into AP1 cells. AP1 is a mutant cell line which does not express functional sodium proton exchangers. It was derived from Chinese hamster ovarian cells (CHO) (102, 109). Stably transfected cell lines were established using LIPOFECTAMINE™ 2000 Reagent (Invitrogen Life Technologies, Carlsbad, CA, USA). Approximately 24 hours prior to transfection, AP1 cells were cultured in 60mm dishes with α-MEM medium (Hyclone, Logan, UT, USA) containing 10% BGS, and 25 mM HEPES without any antibiotics. 10 μg of plasmid was used for each dish of AP1 cells. The plasmids and 20 μl of LF2000 were diluted in 500 μl of Opti-MEM medium separately and incubated for 5 min at room temperature. The solutions were then combined and left to sit at room temperature for 20 min to allow formation of DNA-LF2000 complexes. AP1 cells were washed with phosphate buffered saline (PBS) and changed to α-MEM medium that contained neither antibiotics nor bovine growth serum (BGS). 1 ml of DNA-LF2000 complex solution was added to AP1 cells slowly drop by drop. 10% BGS was added after 4-6 hours and cells were allowed to incubate until the next day. AP1 cells were split into 3 plates at varying dilutions of 1:1000, 1:2000 and 1:2500 in growth medium (10% BGS, 2% penicillin/streptomycin, 0.4 mg/ml gentimicin, 25 mM HEPES). 800 μg/ml of geneticin (G418) was added to the cultures to select for positively transfected cells. Medium containing 800 μg/ml of G418 was changed daily for 3 days, then every other day until colonies began to form. G418 was decreased to 600 μg/ml when AP-1 colonies were visible to naked eyes, and to 400 μg/ml 2 to 3 days

before picking single colonies. Cell colonies were picked using sterile pipettes and transferred to a 12-well plate containing 1.5 ml growth medium with additional 5% BGS and without G418. Medium was changed the next day to growth medium containing 400 μg/ml G418 and fresh medium was provided every 2 to 3 days. When the cells became confluent, they were split into 35 mm dishes and 6-well plates. Cells from 35 mm dishes were harvested to check for NHE1 expression, and cells from 6-well plate were kept as stable cell lines stored in liquid nitrogen tank in CryoTube™ vials (NUNC™ Denmark) for future experiments.

2.9 Preparation of cell lysates from AP1 cells

Cells were harvested from 60 or 35 mm dishes when 80 – 90% confluent. Growth medium was removed by aspiration and cell monolayers were washed with 4^{o}C phosphate-buffered saline. Plates were kept on ice to reduce protein degradation. RIPA Lysis buffer (1% NP-40, 0.25% sodium deoxycholate, 0.1% Triton X-100, 5 mM EGTA, 0.1 mM PMSF, 0.1 mM benzamidine, lab-made protease inhibitor cocktail) was added to AP1 cells for 1 - 3 min. Cells immersed in lysis buffer were scraped with a sterile disposable cell scraper, and the lysates were transferred into clean eppendorf tubes. Cell debris was removed by centrifugation at 14000 rpm for 5 min at 4^{o}C. Supernatants were kept in eppendorf tubes and they were either frozen quickly in liquid nitrogen and stored at -80^{o}C, or prepared for subsequent trypsin treatment and SDS-PAGE.

2.10 SDS-PAGE and Western Blot analysis

10% acrylamide gels were prepared for SDS-PAGE. The loading samples contained cell lysates and 4X SDS-loading buffer (30% glycerol, 3% 2-mercaptoethanol, 6% SDS, 0.13 M Tris pH6.8, 0.133 g/ml bromophenol blue). For expression and surface localization experiments, loading samples were incubated at 37^{o}C for 10 min before loading, and the maximum loading quantity was 60 μl. Samples were allowed to run into the stacking gel for about 40 min at 70 V until the dye front reached beyond the separating gel layer. The voltage was then increased to 120 V and the gel was run for approximately 1 hour until the dye ran out of the gel.

When SDS-PAGE was complete, the stacking gel was cut off and the separating gel containing resolved NHE1 was blotted onto nitrocellulose membrane (Bio-Rad Laboratories, Ontario, Canada) for 2 hours at 450 mA. The membrane was blocked in 10% milk solution (1g/ml milk, tris-buffered solution (TBS)) with agitation for 2 hours at room temperature. Primary antibody, 12CA5 (1:2000 dilution monoclonal mouse anti-HA antibody), was added to probe hemmaglutinnin tagged C-term tail for 2 hours at room temperature or overnight at 4^{o}C with agitation in the presence of 1% milk. After primary incubation, the membrane was washed with TBS 4 times X 15 min . Secondary antibody, GAM (1:10000 dilution Goat-Anti-Mouse), was added and incubated for 1.5 hour at room temperature with 1% milk. NHE1 protein was visualized using the ECL (enhanced chemiluminescence) technique. Nitrocellulose membrane was immersed in 10 ml of ECL reagent (Tris-HCl pH8, 22.5 mM luminol, 6 mM

commaric acid, 0.04% hydrogen peroxide) for 1 min. X-ray films (Fuji medical X-ray film) were processed using a Kodak X-OMAT 2000 M35 processor. ImageJ 1.35 software (National Institutes of Health, Bethesda, MD, USA) was used to quantify band intensities.

2.11 Activity assays

All activity assays were performed on at least two independently made clones of each TMVI cysteine mutant stable cell lines using a PTI Deltascan spectrofluorometer. Experiments were done at 37^{o}C and all solutions and relevant equipment was pre-warmed to 37^{o}C. WT, cNHE1, and TMVI mutants were cultivated on coverslips (THOMAS® Red Label® MICRO COVER GLASSES) in 35 mm dishes until more than 80% confluent. The coverslip was then incubated in 400 μl serum free α-MEM medium containing 1.875 μg/ml 2' - 7'-bis(2-carboxyethyl)-5(6) carboxyfluorescein-acetoxymethyl ester (BCECF-AM; Molecular Probes Inc., Eugene, OR, USA) for 20 min to allow BCECF-AM to permeate through cell membrane. BCECF is a fluorescent dye such that its intensity of fluorescence varies with pH. Extracellular BCECF-AM is non-fluorescent and permeable to the cell membranes. Once it gets inside the cell, it becomes de-esterified to BCECF, fluoresces with varying pH and is impermeable to the membrane. Dual excitation of BCECF was used. BCECF treated cells were excited at 425 nm and 503 nm, and emission was measured at 524 nm. The reason for using a double excitation method was to correct the absolute level of fluorescence which varies with the amount of BCECF absorbed. In order to

measure the activity of NHE1, the cells were transiently acidified using 50mM ammonium chloride (NH_4Cl). Ammonium(NH_4^+) enters the cell and decomposes into ammonia (NH_3) and a H^+. As the small uncharged ammonia can readily diffuse out of the cell more rapidly than ammonium, this shifts the equilibrium to the right and produces even more H^+, thereby inducing intracellular acidosis.

2.11.1 One-pulse assays

In the one-pulse assay for Na^+/H^+ exchanger activity, the cells were plated on coverslips and acidified only once using ammonium chloride. They then recovered in normal sodium containing buffer and NHE1 activity was measured during pH_i recovery. The coverslip was attached to a coverslip holder, placed in a cuvette filled with 2.5 ml normal buffer pH7.3 (135 mM NaCl, 5 mM KCl, 1.8 mM $CaCl_2$, 1 mM $MgSO_4$, 5.5 mM glucose, 10 mM hepes) and left in the fluorometer for 3 min. 50 μl of 2.5 M ammonium chloride was added by pipette to the normal buffer in cuvette and the cells were incubated for another 3 min. The coverslip holder was then immersed in a cuvette containing fresh 2.5 ml sodium free buffer pH7.3 (135mM N-methyl glucamine, 5 mM KCl, 1.8 mM $CaCl_2$, 1 mM $MgSO_4$, 5.5 mM glucose, 10 mM hepes) for 30 seconds. This step allowed the removal of the external ammonium chloride and induced transient intracellular acidification. In the absence of sodium, NHE1 was unable to recover the pHi of cells. The coverslip was returned to normal sodium containing buffer, thus allowing the acidified cells to recover pH via the activity of NHE1. Each measurement of activity was followed by a 3 point pH calibration to calibrate the

amount of fluorescence to pH_i. pH calibration buffers at a pH of 6, 7, and 8 were used (5 mM N-Methyl Glucamine, 135 mM KCl, 1.8 mM $CaCl_2$, 1 mM $MgSO_4$, 5.5 mM glucose, 10 mM HEPES, pH adjusted with KOH and HCl). pH calibration buffer contained 10 mM nigericin, which acts as an ionophore to equilibrate K^+ and H^+ across the cell membrane. Activity traces were calibrated using the pH calibration curves. The initial rate of recovery during the first 20 seconds was used to calculate the activity of NHE1 (Figure 4).

2.11.2 Two-pulse assays: EMD 87580 and MTSET/MTSES treatments

Two-pulse Na^+/H^+ exchanger assays consisted of two ammonium chloride acidification pulses with a chemical treatment in the second pulse. EMD87580 (N-(4,5-Bis-methansulfony-2-methyl-benzoyl) guanidine) is a specific inhibitor of NHE1 activity. MTSET ([2-(Trimethylammonium) Ethyl] Methanethiosulfonate) and MTSES ([2-(Sulfonylethyl)]Methanethiosulfonate) are sulfhydryl reactive compounds that are able to form covalent bonds with water soluble cysteine side chain. MTSET is positively charged and MTSES is negatively charged. Formation of covalent interactions with a protein translocation pore cysteine side chain with MTSET or MTSES may inhibit the activity of cation transport in NHE1. The chemical structure of MTSET and MTSES are similar to a hydrated Na^+.

In order to test how the treatments (EMD87580, MTSET and MTSES) affected NHE1 activity the two pulse assay was used (Figure 5). This allowed comparison of the first untreated pH recovery to the second pH recovery of

treated cells. The first recovery in the two pulse assay is done identically to a one pulse assay, where the cells were acidified in ammonium chloride and recovered in normal buffer. The second recovery in the two pulse assay, is normally almost identical to the first when done in the absence of other reagents. To test the inhibitory effects of EMD87580 on cNHE1, in the second pulse EMD87580 was added to a final concentration of 10 μM in the normal buffer after pH recovery. The cells were incubated with EMD87580 for 3 minutes in the fluorometer, and ammonium chloride was then added. After another 3 minutes, the cells were incubated in sodium free buffer containing 10 μM EMD87580 for 30 seconds. The cells were then allowed to recover in the normal sodium containing buffer in the presence of 10 μM EMD87580. A three point pH calibration was conducted at the end of the activity assay (Figure 17).

Treatment of cells with MTSET and MTSES was also carried out in a two pulse assay. The first half was identical to the one pulse assay. Either MTSET or MTSES was then added to normal buffer to 10 mM final concentration after the first acidification was recovered. The cells were incubated in MTSET or MTSES for 10 minutes, and then incubated in normal buffer solution containing 50 mM ammonium chloride for 3 minutes. The incubation buffer was then changed to sodium free solution for 30 seconds to induce intracellular acidification. Finally, the cells were incubated in normal buffer for a second pH recovery, followed by a three point pH calibration.

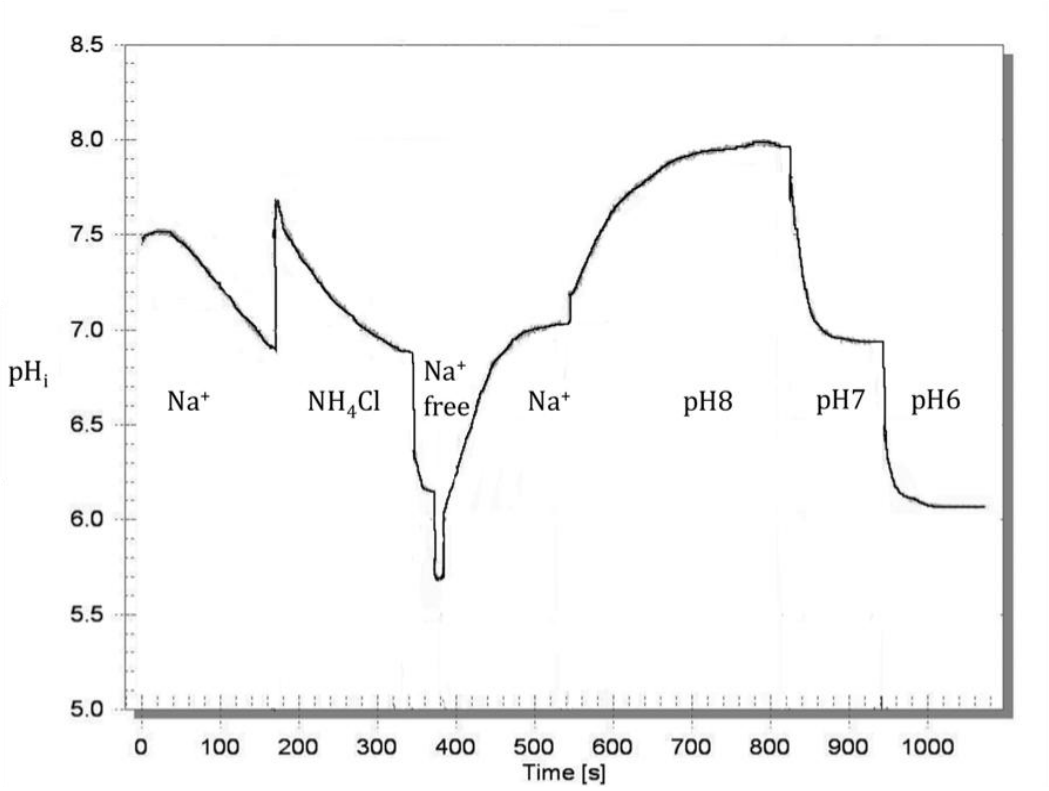

Figure 4. Sample of activity trace of an one-pulse Na^+/H^+ exchanger assay. The trace represents changes in pH_i occurring over time in AP1 cells during one-pulse Na^+/H^+ exchanger assay. The x-axis illustrates the time course of experiment, and the y-axis corresponds to pH_i. Initially, cells are immersed in normal buffer. Adding NH_4Cl to the buffer increases pH_i. Removing Na^+ and NH_4Cl from incubation buffer induces a transient intracellular acidification. In the presence of Na^+, NHE1 returns pH_i back to normal. At the end of an activity trace, a three-point calibration is done using buffers containing nigericin at pHs 8, 7 and 6.

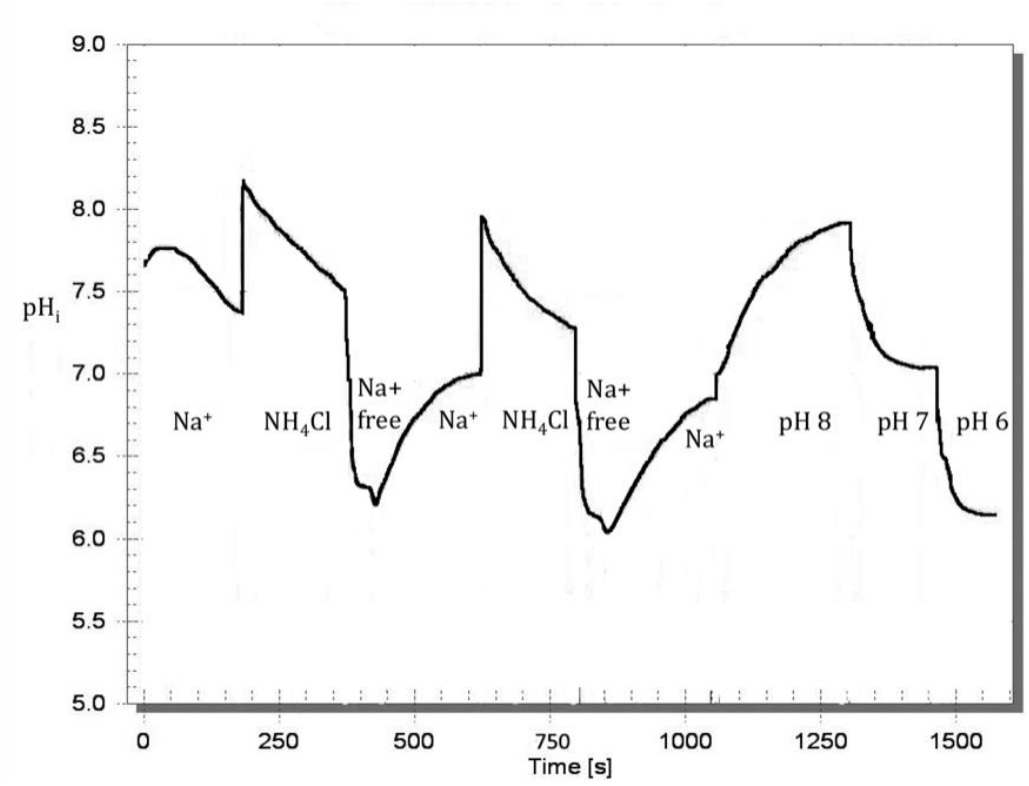

Figure 5. Sample of activity trace of a two-pulse Na^+/H^+ exchanger assay. The trace represents changes in pH_i occurring over time in AP1 cells during a two-pulse assay. The x-axis illustrates the time course of experiment, and the y-axis corresponds to pH_i. Two-pulse assay consists of two consecutive intracellular acidification for the comparison of the first and second pH recovery curves. Initially, cells are immersed in normal buffer. Adding NH_4Cl to the buffer increases pH_i. Removing Na^+ and NH_4Cl from incubation buffer induces a transient intracellular acidification. In the presence of Na^+, NHE1 returns pH_i back to normal. A second acidification is initiated by another NH_4Cl incubation. Removal of Na^+ rapidly induces a decrease in pH_i. Recovery of the pH occurs in the presence of Na^+. At the end of an activity trace, a three-point calibration is done using buffers containing nigericin at pHs 8, 7 and 6.

2.12 Analysis of surface localization

To examine the targeting of NHE1 to the cell surface, cells were grown to 50 – 70% confluence in 60mm dishes. The plates were placed on ice, washed once with 4^{o}C PBS followed by a second wash with 4^{o}C borate buffer pH9 (154mM NaCl, 7.2 mM KCl, 1.8 mM $CaCl_2$, 10 mM boric acid). 3 ml of freshly made sulpho-NHS-SS-Biotin (Pierce Chemical Company, Rockford, IL, USA) at a concentration of 0.5 mg/ml in borate buffer was added to each plate and cells were incubated for 30 min at 4^{o}C. Cells were then washed 3 times with cold quenching buffer pH8.3 (192 mM glycine, 25 mM Tris) on ice. Solubilization of cells was achieved by addition of 500μl IP lysis buffer pH7.5 (1% (w/v) deoxycholic acid, 1% (w/v) Triton X-100, 0.1% (w/v) SDS, 150 mM NaCl, 1 mM EDTA, 10 mM Tris/Cl, 0.1 mM PMSF, 0.1 mM Benzamidine, and lab-made protease inhibitor cocktail). Cell debris was removed by centrifugation at 16000g at 4^{o}C for 20 min. Supernatants were transferred into two equal 200 μl fractions in eppendorf tubes, to a "Total" fraction and an "Unbound" fraction. In the unbound fraction, 50 μl of immobilized strepavidin resin was added to bind the biotin labelled proteins. Unbound fractions were then incubated at 4^{o}C overnight with gentle rocking. Supernatants were collected the following day by centrifugation at 16000 g for 2 min. 25 μl of the total fraction and 28 μl of unbound fraction were loaded on 10% acrylamide gels for SDS-PAGE. NHE1 was detected by western blotting, and quantified using Image J software.

2.13 Analysis of protein expression levels

Equal amounts of protein (75 μg) were loaded in SDS-PAGE to measure NHE1 expression. Cell lysates were prepared for SDS-PAGE on the same day. Protein concentrations were measured at least 3 times using BioRad DC^{TM} protein assay kit. The NHE1 bands were detected by western blotting, as described above. Three to four repeats were done for each gel. Quantification was done using Image J software.

2.14 Limited trypsin digestion of NHE1

Cell lysates were prepared as described above using RIPA lysis buffer, with the exception that proteinase inhibitors PMSF, benzamidine and protease cocktail were not added. Trypsin (phenylalanyl chloromethyl ketone-trypasin, Sigma, St., Louis, MO) was prepared and dissolved in TE buffer. Equal amounts of proteins (100 μg) from cell lysates were treated with trypsin at different trypsin:protein ratios (1:1500, 1:2000, 1:2500, 1:3000) and incubated at 37^{o}C for 5 min. The reaction was terminated by addition of SDS-PAGE loading buffer followed by boiling at 100^{o}C for 5 min. Samples were resolved by SDS-PAGE and NHE1 detected by western blot analysis.

2.15 Statistics

All activity assays and surface localization results were produced from at least 6 repeats. Protein expression levels were determined at least 3 times. Statistical significance was calculated using Mann-Whitney-Wilcoxon test.

Chapter III

Results

A version of this chapter on NHE1 TMVI cysteine mutations also appears in the Journal of Biological Chemistry (2010) 285:36656-65. Jennifer Tzeng, Brian Lee, Brian Sykes and Larry Fliegel. All data in this chapter is performed by Jennifer Tzeng.

3.1 Characterization of expression: TMVI cysteine mutants

NHE1 transmembrane segment VI (Asn227 – Ile249) was proposed to be involved in the cation transport activity based on the homology model structure with *E. coli* NhaA (45, 67). Cysteine scanning mutagenesis was used to study TMVI to specifically investigate the contribution and function of each residue. All TMVI cysteine mutant plasmids were successfully transfected in AP1 cells and the expressed NHE1 protein was detected by SDS-PAGE and western blotting. At least two clones of each mutant cell lines were characterized. Expression levels of each TMVI cysteine mutants were determined by densitometric analysis (Figure 6). NHE1 was detected by blotting against the HA-tag on the C-terminus. NHE1 appears as two forms on western blots: the mature NHE1 is glycosylated on its first extracellular loop and has a higher molecular weight at around 105 – 110 kDa, whereas the immature form of NHE1 is partially or non-glycosylated with a molecular weight of approximately 85 -95 kDa (20, 39). AP1 cells did not contain any detectable HA-tagged NHE1 protein (Figure 6). Of the mutant proteins, Asn227Cys and Ala236Cys displayed the greatest decrease in expression to less than 30% of cNHE1 levels. Ile233Cys and Pro239Cys also had severe reductions in expression to 60% and 40% of cNHE1 levels respectively. Interestingly, there were several residues that exhibited significantly higher expression than cNHE1 (Gly231Cys, Ser232Cys, Ile234Cys, Ser235Cys, Val237Cys, Asp238Cys, Leu243Cys, Ala244Cys, Val245Cys, and Phe246Cys). One of the most intriguing findings from the expression

experiments was that only the immature form of NHE1 was observed in Pro239Cys and Glu247Cys mutations.

3.2 Surface localization of TMVI cysteine mutants

Membrane proteins are usually synthesized in the endoplasmic reticulum, processed further in the golgi bodies, and sent to membrane locations via vesicles. Previous studies have found that mutations in NHE1 may disrupt this synthesis and transport network, which caused intracellular retention of the mutant protein (120, 133). The surface localization of TMVI cysteine mutants was therefore measured. Cell lysates, total and unbound protein, representing total and intracellular proteins, were loaded in equal amounts for SDS-PAGE and western blotting. NHE1 bands were blotted by anti-HA tag antibodies and visualized by ECL. The amount of fully glycosylated and partially glycosylated NHE1 were calculated and compared using ImageJ 1.35 software (Table 2). A background control of nonspecific protein binding to strepavidin-agarose beads was examined. Results (Figure 7) indicated that there was no significant nonspecific binding of unlabelled proteins. In general, the mature form of wild type, cysteineless, and mutant NHE1 proteins at 110 kDa were mostly targeted to the plasma membrane (70% to 80%). The immature NHE1 remained mainly intracellular, only around 15% to 25% was surface localized. For Pro239Cys and Glu247Cys mutations, surface localization of mature NHE1 was not measureable, however they had a similar percentage of partially glycosylated NHE1 expressed on the surface. A few mutants had less than 30% of mature NHE1 surface localization, they are Leu229Cys, Ile234Cys, Ser235Cys, Ala241Cys, Val242Cys, and Val245Cys.

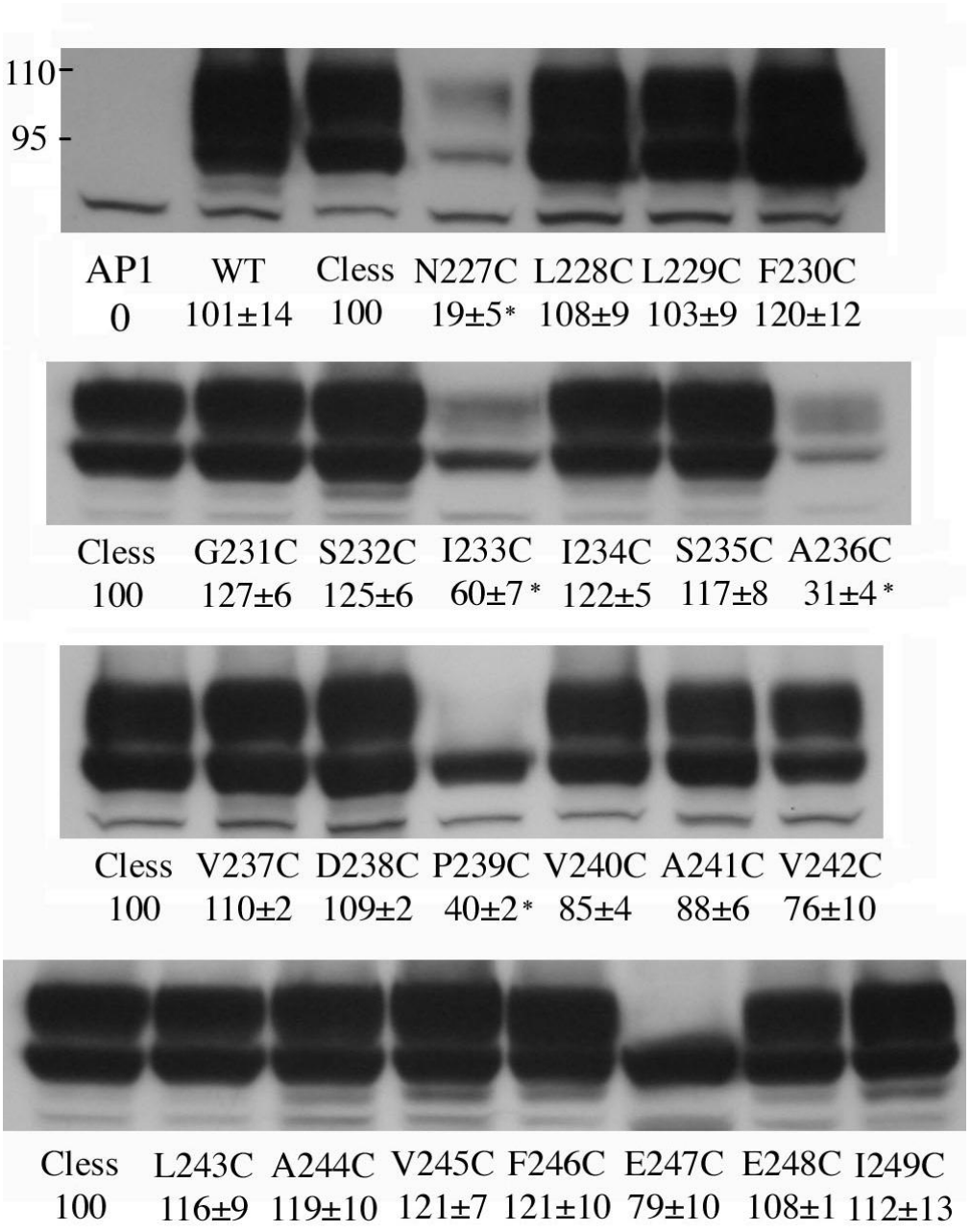

Figure 6. NHE1 expression of TMVI cysteine mutants in AP1 cells. Western blot of whole cell extracts of WT NHE1, cNHE1 control, and TMVI cysteine mutants. NHE1 was probed using anti-HA antibodies. Each lane contained 75μg of total protein. Two bands of NHE1 were detected: a mature form at 110kDa and an immature form at 95kDa. The amount of expression was evaluated from densitometric analysis of both forms of NHE1. AP1 cells did not express endogenous NHE1. The results are a mean of 3 – 4 experiments. * indicates mutants with significantly lower expression than cNHE1 at $P<0.05$.

Substitution of Ile233 and Leu243 to cysteines, displayed increases of 10% to 15% in surface localization of the mature NHE1 form.

3.3 Activity assays of TMVI cysteine mutant containing cells

3.3.1 One-pulse assay

The cation transport activity of NHE1 TMVI mutant stable cell lines was determined using the fluorescent dye, BCECF-AM as described above. A one-pulse assay was carried out to determine whether the TMVI cysteine mutants had enough activity for further analysis using MTSET and MTSES. At least two independent clones of each type of TMVI mutation were used. Figure 8 depicts the raw Na^+/H^+ exchanger activity in black bars and normalized activity with expression levels and mature NHE1 surface localization levels is shown by gray bars. Untransfected AP1 cells had no Na^+/H^+ exchanger activity; therefore they could not recover from intracellular acidification. A few residues that were mutated to cysteine exhibited very low NHE1 activity, less than 15% of cNHE1 control (Pro239Cys, Asp238Cys, and Glu247Cys). Asn227Cys, Ile233Cys, Ala236Cys, Leu243Cys, and Glu248Cys also had low activity, from 15% to 40% of cNHE1. After correcting the activities for expression and surface localization, Asn227Cys, Ala236Cys, Ala241Cys, and Val242Cys exhibited activity close to cNHE1 activity. The low activities of Asn227Cys and Ala236Cys were mostly contributed by their low expressions, whereas Ala241Cys and Val242Cys had reductions in expression and surface localization. There were two mutants, Ser235Cys and Ile249Cys, with significantly higher activities than cNHE1. When normalized, Ser235Cys had elevated activity due to its lower surface localization.

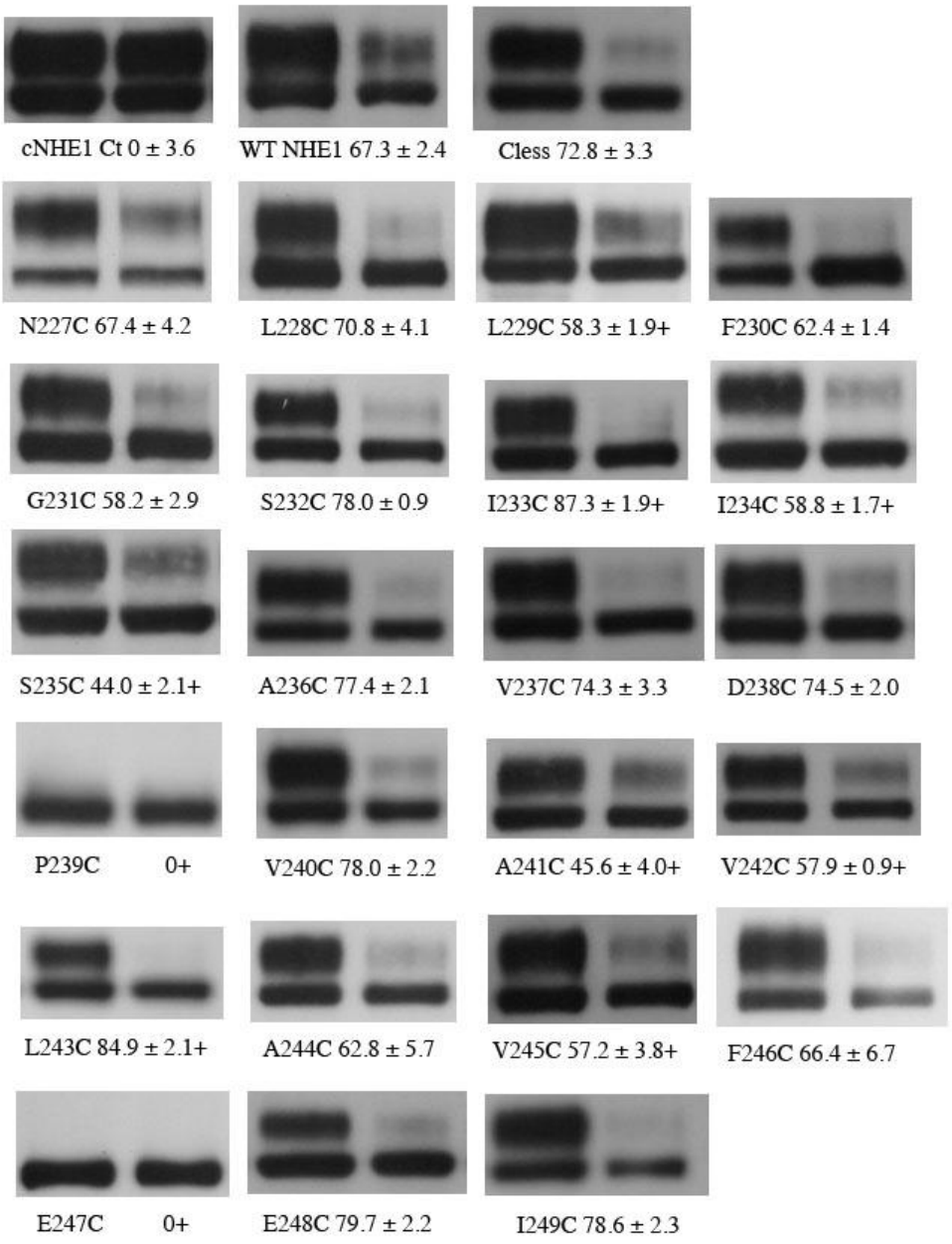

Figure 7. Surface localization of NHE1 TMVI cysteine mutants. Equal amounts of total protein fraction and unbound fraction of WT NHE1, cNHE1 control, and TMVI cysteine mutants were assessed by western blotting with anti-HA antibody. The amount of surface localized NHE1 was calculated from densitometric analysis by taking the (total protein) – (unbound protein) = (membrane surface localized protein). AP1 cells did not express HA-tagged NHE1. + indicates mutants with significantly different surface localization than cNHE1 at $P<0.05$. Results are mean ± S.E. n = at least 6 experiments.

However Ile249Cys activity was reduced, since it exhibited increases in both expression and surface localization.

3.3.2 Two-pulse assay with MTSET and MTSES treatments

TMVI cysteine mutants with uncorrected activity that was higher than 15% of wild type, were considered for MTSET and MTSES treatments. Asp238Cys, Pro239Cys, and Glu247Cys were essentially inactive, therefore any slight inhibition caused by the treatments would not be detectable. MTSET and MTSES are sulfhydryl reactive chemicals commonly used to examine externally accessible amino acid residues (31, 42, 137). The binding of MTSET or MTSES to accessible cysteines in the transmembrane segment that lies along the translocation pore, may block cation passage. A two-pulse assay was carried out to characterize the effects of MTSET and MTSES on TMVI cysteine mutations (Figure 9). Phe161Cys mutant in TMIV of NHE1 was found to be sensitive to both MTSET and MTSES in our lab previously; therefore it was used as a positive control for treatments (117). Asn227Cys, Ile233Cys, and Leu243Cys exhibited the greatest inhibition when treated with MTSET (Figure 9, 10). pH recovery was almost completely abolished by MTSET treatment and resembled the effects of EMD87580 treatment (Figure 17). Several TMVI cysteine mutants Phe230Cys, Gly231Cys, Ala236Cys, Val237Cys, Ala244Cys, Val245Cys, and Glu248Cys were sensitive to MTSET treatment to a lesser degree. Interestingly, only the positively charged MTSET affected the TMVI cysteine mutants. There was a noticeable pattern of residues that were sensitive to MTSET. Starting from Asn227Cys, MTSET inhibited amino acids that were three to four residues apart.

The neighboring residues of Leu243Cys were slightly affected by MTSET as well. Similar occurrences were observed in functional investigation on other transmembrane segments of NHE1 (28, 69, 103, 120). MTSES had no significant inhibition on any residues, yet there was a slight increase in activity when treated to Val242Cys.

3.4 Characterization of expression: critical residues of TMVI mutants

Residues mutated to cysteines that were either inactive or sensitive to MTSET treatment were further investigated. The activity of mutants Asn227Cys, Ile233Cys, and Leu243Cys were almost abolished completely by MTSET. The Glu247Cys mutant was essentially inactive. Glu248Cys exhibited ~55% uncorrected activity and was partially inhibited by MTSET. Therefore nine more mutations were created to replace these residues in the background of wild type NHE1 protein. Hydrophilic Asn227 was mutated to an Ala which has a small side chain, a Gln with longer hydrophilic side chain, and a positively charged Arg. Ile233 and Leu243 were mutated to alanine to remove the contribution of long hydrophobic side chains of Ile and Leu. Glu247 and Glu248 were mutated into similarly charged but smaller Asp and a polar Gln side chain removing the free negatively charged carboxyl of the amino acid. Expression levels of NHE1 mutants were examined by SDS-PAGE and Western blotting. In general, the mutants expression varied compared to wild type NHE1 (Figure 11). Asn227Ala, Glu247Asp, Glu247Gln, and Glu248Asp exhibited slightly elevated NHE1 expression by 10%. Mutation of Asn227 to Arg reduced expression of the mature NHE1 drastically. Of all the mutants, Ile233Ala displayed the lowest expression

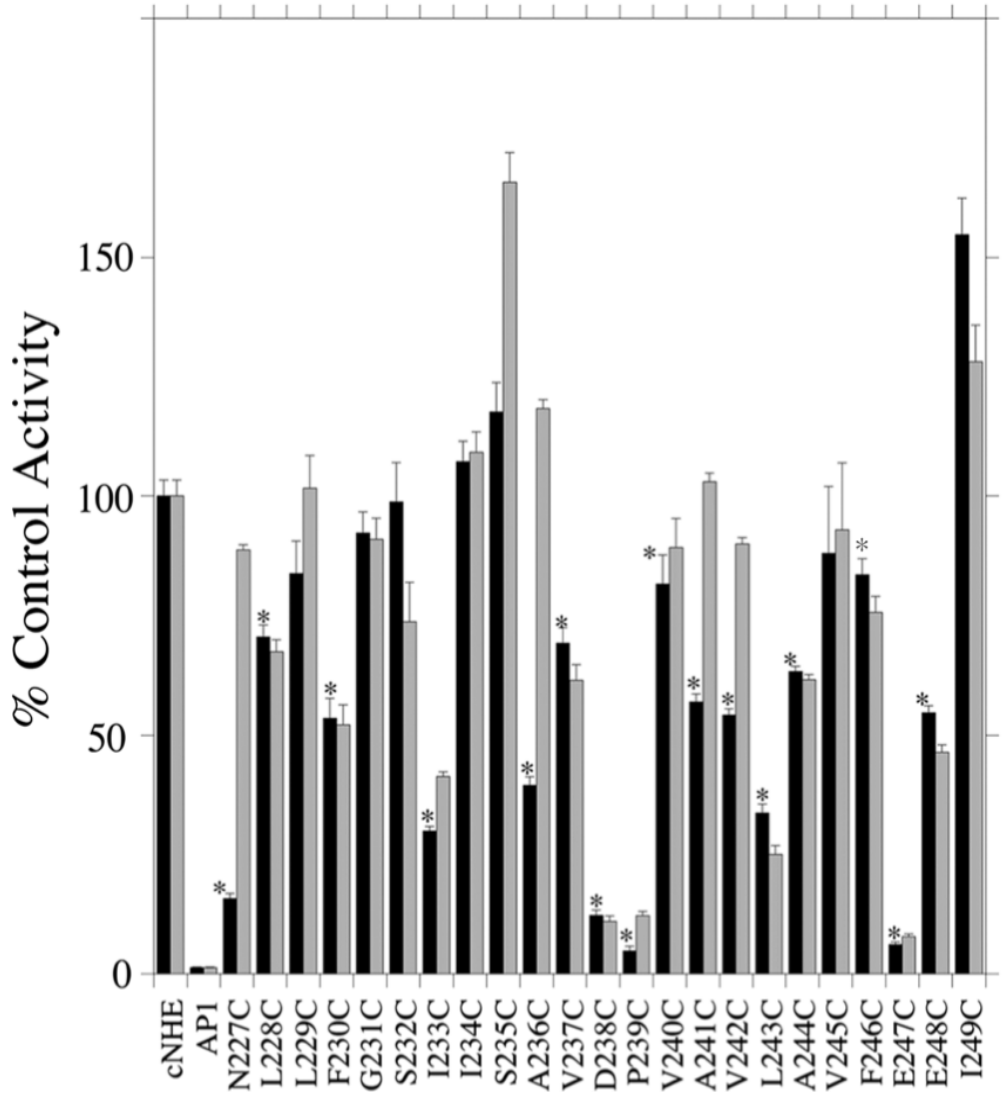

Figure 8. NHE1 activity of TMVI cysteine mutants determine by one-pulse assay. The activities of cNHE1 control, AP1, and TMVI cysteine mutants were determined using a one-pulse assay. The rate of recovery of cNHE1 was set at 100% and TMVI cysteine mutants' recovery rates were compared to that of cNHE1. Results are mean +/- SE (n = at least 6 determinations). Uncorrected NHE1 activities are represented as black bars and corrected activities are represented as gray bars. * uncorrected mutant activities that is significantly lower than that of cNHE1 at $P < 0.05$.

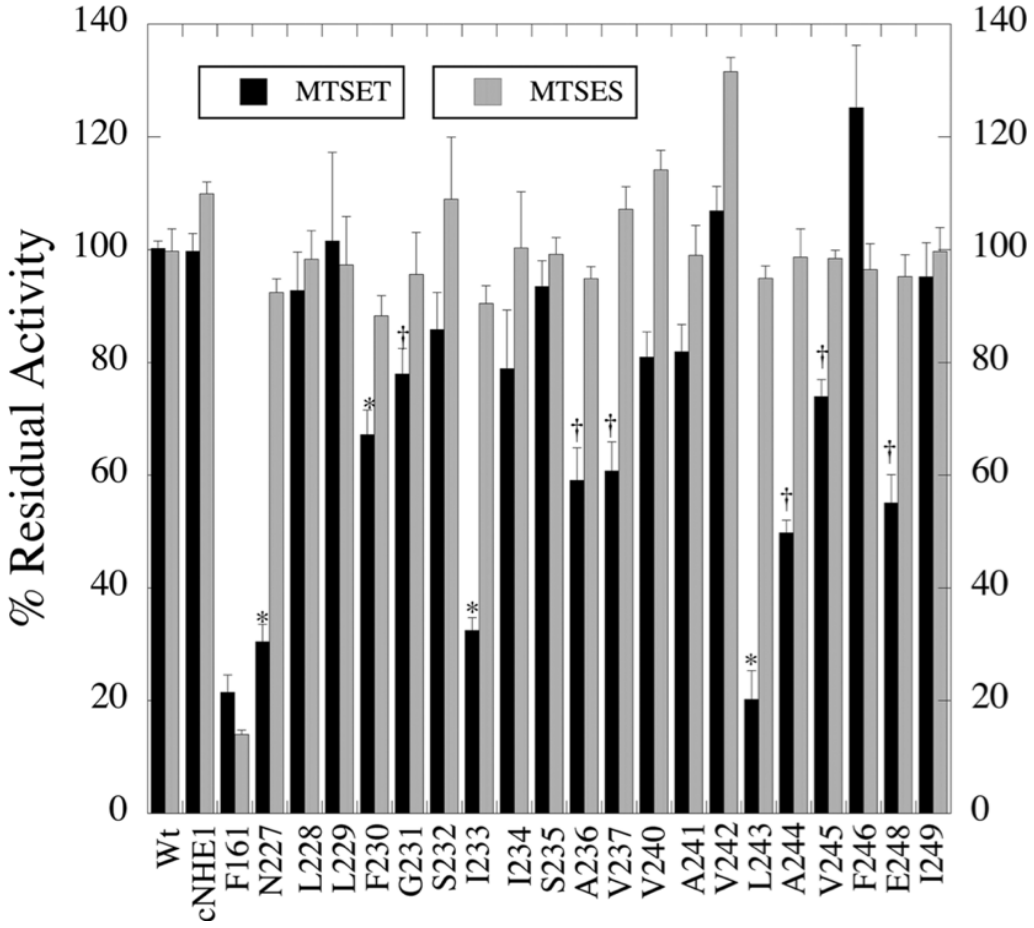

Figure 9. Residual NHE1 activity of TMVI cysteine mutants from MTSET/MTSES treatment. Summary of effects of 10 mM MTSET/MTSES treatment on activities of cNHE1 control, AP1, and TMVI cysteine mutants. Black bars represent MTSET treatments and gray bars are MTSES treatments. Results are mean activities (n = at least 6 determinations) of the % second recovery relative to the first. * and † indicate TMVI cysteine mutant residual activities significantly lower than the first at $P < 0.05$ and $P < 0.001$ respectively.

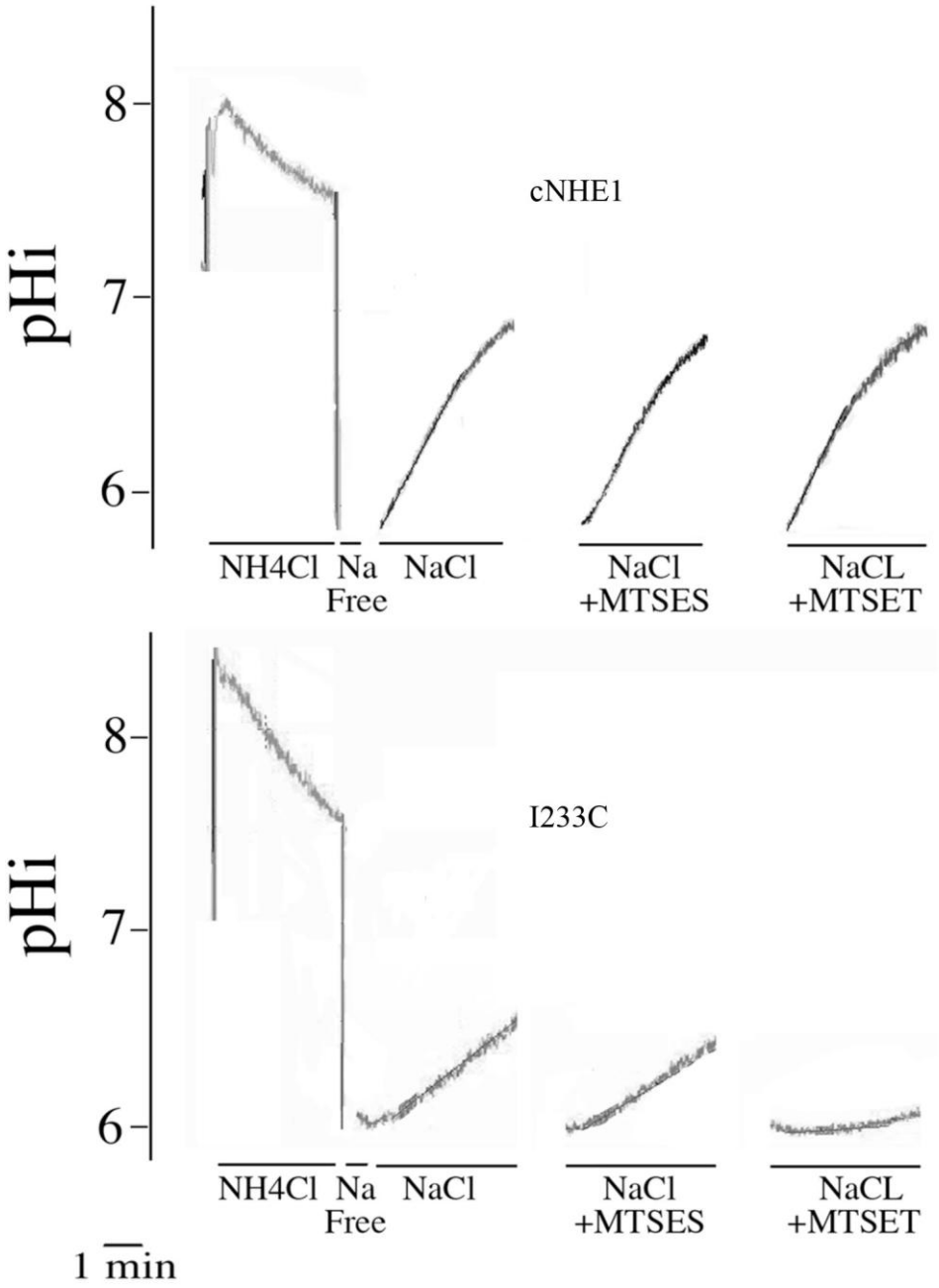

Figure 10. Effect of MTSET and MTSES on activity of cNHE1 and I233C. The activities of cNHE1 and I233C were determined in two-pulse assays. The recoveries from second acidification were shown in the absence of sulfhydryl reactive reagents, and treatments with MTSES and MTSET. NH_4Cl, treatment with ammonium chloride; Na Free, treatment with Na^+ free buffer to induce acidosis; NaCl, recovery from acidosis in NaCl containing buffer.

levels at 44% of wild type. Whereas Leu243Ala and Glu248Gln had expression levels reduced to ~90% and ~75% of control NHE1 respectively.

3.5 Surface localization of critical TMVI mutants

The surface localization of the nine TMVI mutants was investigated as previously described in the methods section. The surface processing of fully glycosylated and immature forms of NHE1 were quantified (Table 3). Surface localization of the upper band from NHE mutants showed less variation compared to the control (Figure 12). Asn227Arg only exhibited ~29% of mature NHE1 targeted to the membrane surface, whereas the immature bands remained constant as intracellular. Ile233Ala and Glu248Gln displayed ~20% higher localization of mature NHE1 to the surface. There was a ~10% significant reduction of Glu248Asp mutant on the plasma membrane.

3.6 Activity of critical TMVI mutants

The Na^+/H^+ exchanger activities of nine TMVI mutants were determined by one-pulse assays. Control wild type NHE1 activity was set to 100% and all the mutant activities were expressed as a percent of control. Figure 13 illustrates the uncorrected NHE1 activities in black bars and the corrected activity in gray bars, which represent activity normalized by expression and surface localization levels of the mature NHE1. Several mutants, (Asn227Arg, Ile233Ala, and Leu243Ala) were almost inactive and had almost no pH recovery after intracellular acidification. Asn227Ala exhibited ~75% of control activity. Asn227Asp and

Glu248Gln were less than 40% active. Correcting the raw activities for protein expression and targeting, did not revert activity back to wild type NHE1 level.

3.7 Limited trypsin digestion on NHE1 with mutated residues

Of the nine new TMVI mutations, Ile233Ala, Leu243Ala, Glu247Asp, and Glu248Gln were chosen for further investigation to determine the nature of the defect in NHE1 activity. Limited trypsin digestions were carried out to reveal changes in protein conformation (85, 88). Cell lysates were treated with trypsin for a limited amount of time (5 min) and at different ratios of trypin:protein (1:1500 to 1:3000) to produce fragments of NHE1 protein to enable evaluation of digestion patterns. Control digestions were done simultaneously with the mutants to make experimental results more uniform. The results (Figure 14) showed that there was no significant difference between the digestion pattern of NHE1 control, Glu247Asp and Ile233Ala mutant proteins (Figure 14). Glu248Gln displayed a high sensitivity to trypsin, and most of the immunoreactive NHE1 bands disappeared even at the lowest trypsin:protein ratio of 1:3000. Leu243Ala was also more susceptible to trypsin hydrolysis compare to WT NHE1. Most of the bands were digested in Leu243Ala mutant at 1:2000 trypsin:protein ratio treatment. There was no appearance of additional bands due to trypsin digestion. NHE1 was probed using anti-HA antibodies which detected the HA-tag on the C-terminal tail, therefore we were not able to detect any changes in N-terminal digested fragments.

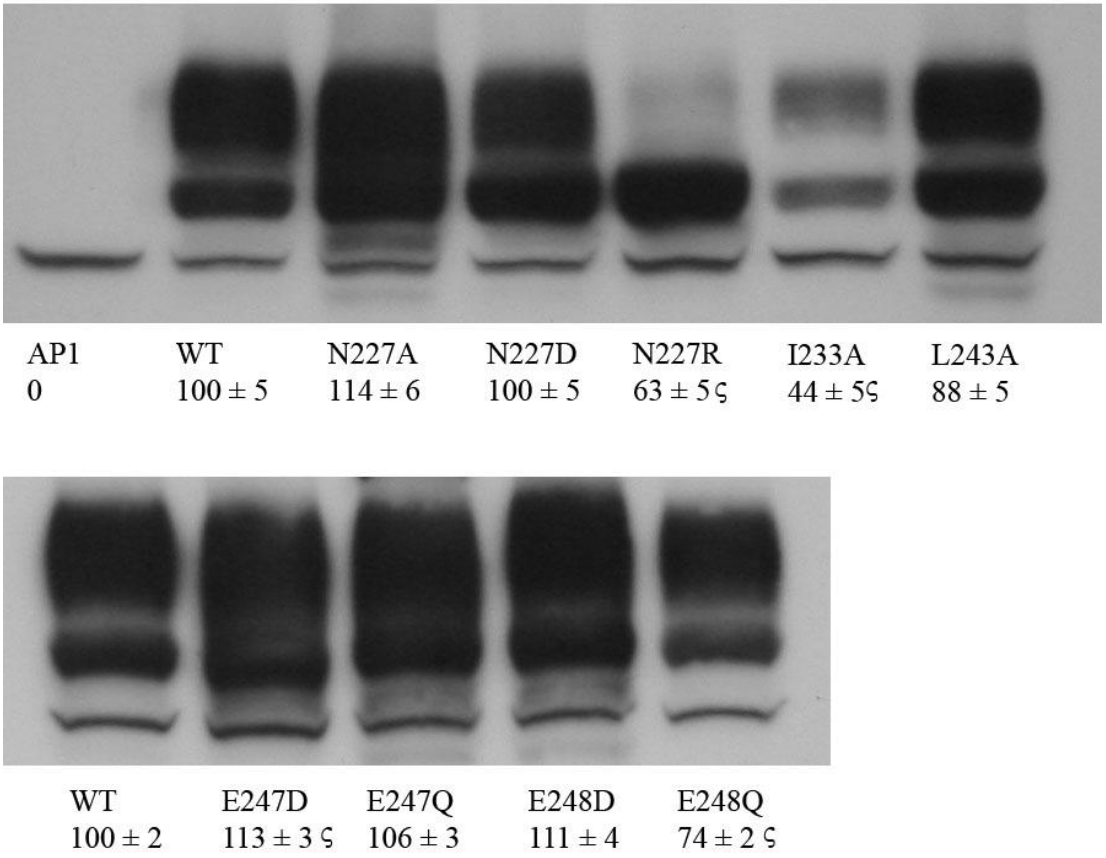

Figure 11. NHE1 expression levels of mutants of critical residues in TMVI. Western blot analysis of whole cell extracts of WT NHE1, and TMVI mutants. NHE1 levels were examined using anti-HA antibodies. Each lane contained 75μg of total protein. Two bands of NHE1 were detected: Mature form at 110kDa and immature form at 95kDa. The amount of expression was evaluated from densitometric analysis of both forms of NHE1. AP1 cells did not express HA-tagged NHE1. The results are a mean +/- SE of 3 experiments. ς indicates mutants with significantly different expression than WT NHE1 at $P<0.05$.

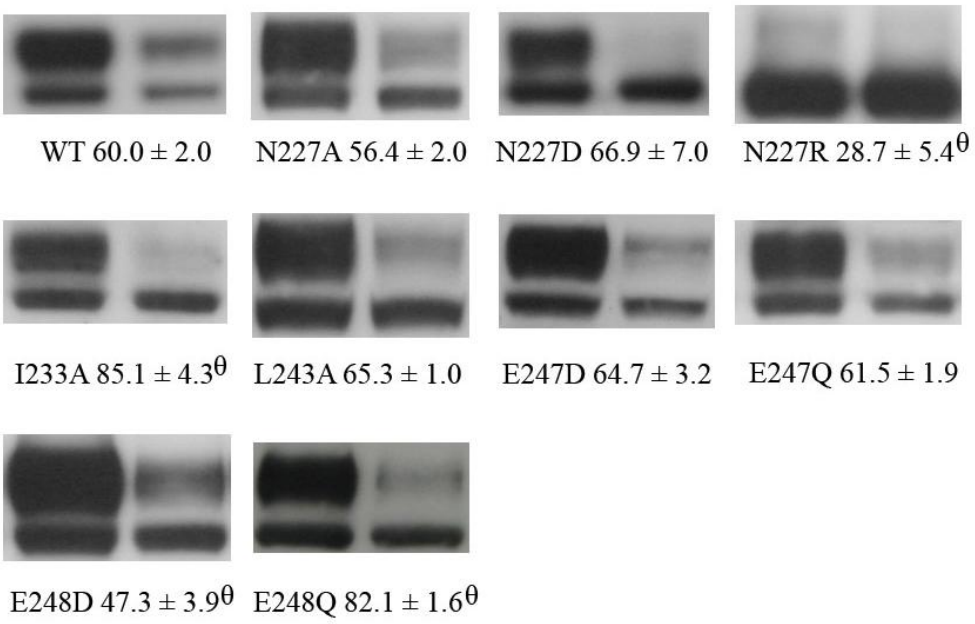

Figure 12. Surface localization of NHE1 proteins with mutations in critical residues of TMVI. Equal amounts of total protein fraction and unbound fraction of WT NHE1, control, and TMVI mutants were assessed by western blotting with anti-HA antibody to probe NHE1. The amount of surface localized NHE1 was calculated from densitometric analysis by taking the (total protein) – (unbound protein) = (membrane surface localized protein). Control AP1 cells did not express HA-tagged NHE1. θ indicates mutants with significantly different surface localization than cNHE1 at $P<0.05$. Results are mean +/- S.E. n = at least 6 experiments.

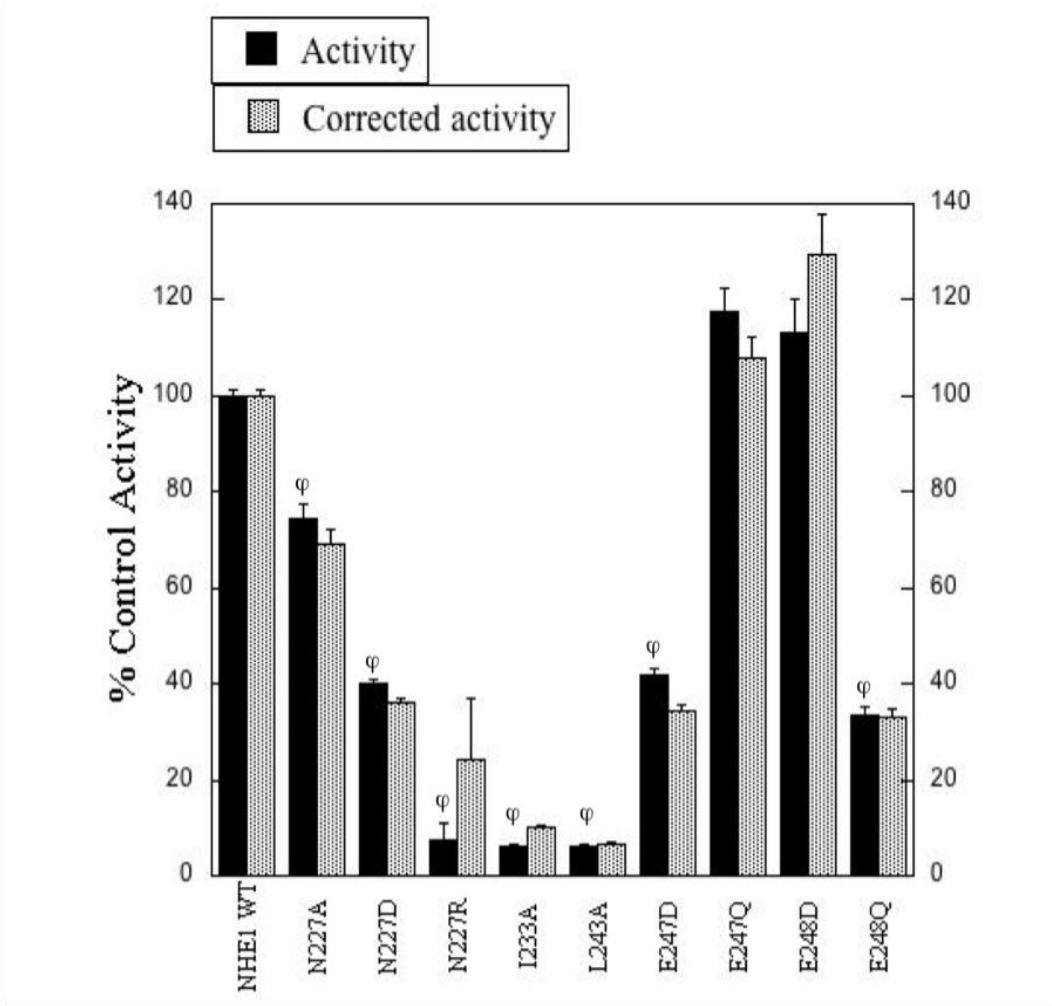

Figure 13. NHE1 activity of TMVI critical residue mutant proteins. The activities of NHE1 WT control, and TMVI mutants were determined by one-pulse assays. The rate of recovery in NHE1 WT was set at 100% and TMVI mutants' recovery rates were normalized to NHE1 WT. Results are mean +/- S.E. (n = at least 6 determinations) of uncorrected NHE1 activities or NHE1 activity corrected for expression levels and targeting represented as gray bars. φ indicates raw TMVI mutant activities that are significantly lower than that of WT NHE1 at $P < 0.05$.

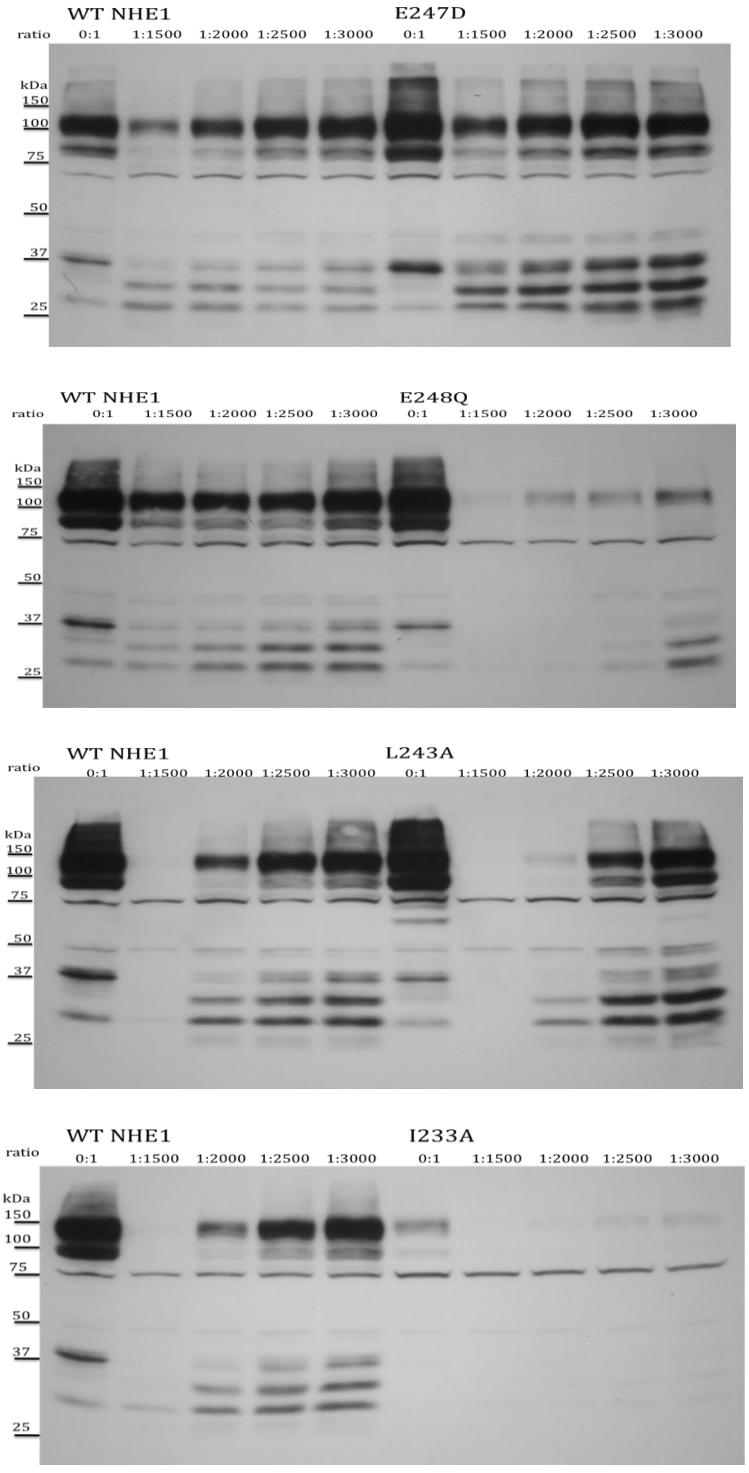

Figure 14. Limited trypsin digestion of selected TMVI mutants. Western blots of WT NHE1, Glu247Asp, Glu248Gln, Leu243Ala, and Ile233Ala whole cell lysates treated with trypsin:protein ratios of 0:1, 1:1500, 1:2000, 1:2500, and 1:3000 as indicated.. The pattern of NHE1 digestion was detected using anti-HA antibodies. Similar results were reproduced for at least two times.

Chapter IV

Discussion

A version of this chapter on NHE1 TMVI cysteine mutations also appears in the Journal of Biological Chemistry (2010) 285:36656-65. Jennifer Tzeng, Brian Lee, Brian Sykes and Larry Fliegel.

4.1 Analysis of TMVI cysteine mutant activity

In this work I characterized the functional characteristics of amino acids 227-249 of the NHE1 isoform of the Na^+/H^+ exchanger. These residues are purported to be either TMVI (132) or TM4 (67) of the protein. This TM segment has not been well studied earlier, but molecular modeling by Landau *et al.* (67) suggested that it may be an important pore lining segment, critical in activity of the protein. Cysteine scanning mutagenesis was performed to examine the pore lining properties of TMVI. All of the amino acids of TMVI from Asn227 to Ile249 were mutated to Cys in the background of the cysteineless protein that we have earlier shown is fully functional (120). Mutations to cysteine reduced the activity of many residues. For the cysteine mutations at residues Asp238, Pro239 and Glu247, their activities were reduced so greatly (less than 15%) that it was not possible to assay these mutants further in MTSET/MTSES treatments. For 12 other cysteine mutants, the activity was reduced but was measurable reliably. We have found that some TM segments, TMIV (36) and TMIX (103) are more tolerant of mutations to cysteine. Whereas TMXI (69) appear to be intolerant of changes.

One-pulse activity assays of cNHE1 and TM VI cysteine mutants were corrected with their relative protein expression and surface localization. Asn227Cys, Ala236Cys, Ala241Cys, and Val242Cys activities have returned to the cNHE1 control level after normalization. This indicated that these mutant proteins were functional, but were not expressed or processed properly. The Asn227Cys and Ala236Cys lower protein expression levels mainly contributed to

the decrease in the cation transport activities. Whereas Ala241Cys and Val242Cys reduced activities were reflected by decreases in protein expression and surface localization. Ile233Cys, Leu243Cys, and Glu248Cys mutants did not exhibit wild type activity after normalization, indicating that the lost of activity was due to hindered cation transport.

Mutation of Pro239 and Glu247 to cysteine residues caused expression of the mature form of NHE1 to decline and expression was predominantly of the immature form of NHE1 that remained intracellular (Figure 6 and 7). The results indicate that the immature and intracellular form of NHE1 is unable to correct intracellular acidosis in AP1 cells. Many mutations in the transmembrane segments of NHE1 also cause immature protein expression. Similar findings are noted in other studies of NHE1 TM segments (TMIV, TMVII, TMIX, and TMXI). Six of the twenty-three residues from TMIV, and seven of the twenty-two from TMXI cysteine mutants express the immature form of NHE1, which is intracellular and essentially inactive (28, 69, 103, 120). The TMXI Tyr454Cys mutant was shown to be retained in the endoplasmic reticulum by immunofluorescence microscopy. Interestingly, the intracellular Tyr454Cys can be rescued to the plasma membrane by having a second point mutation at Cys8Ala in the N-terminal (133).

The Asp238Cys mutant had little activity but showed similar expression and surface localization to the cNHE1 control. This suggests that Asp238 is essential for the cation exchange activity of NHE1, and that the decreased activity we observed is not due to less protein or inappropriate protein targeting to the cell

surface. In the homology model structure of NHE1 (67), Asp238 is positioned at the centre of the cation translocation pore. It corresponds to the Asp133 in EcNhaA (45, 67). The crystal structure of *E. coli* NHaA was determined at 3.45Å and revealed a cation translocation pore constrained by transmembrane helices (45). Two transmembrane helices of NhaA are discontinuous, TM4 and TM11 have a helix – loop – helix structure, which cross over at the loop region with each other. Between the helix dipoles of TM4 and11 is a negatively charged Asp133. This residue compensates for the positively charged discontinuous N-terminal helix dipoles. Therefore, the corresponding Asp238 residue in NHE1 may be crucial in compensating for the charge of similar repulsive helix dipoles (67). Another possibility is that Asp238 may serve as a titratable residue in the centre of the translocation pore (67).

4.2 Critical residues of TMVI that line the cation transport pore

When mutated to cysteine, several amino acids of TMVI (amino acids 227-249) were exquisitely sensitive to reaction with MTSET, as determined in two-pulse assays. Of the 20 cysteine mutants that were active, treatment with MTSET resulted in inhibition in 10 amino acids positions. This made TMVI more susceptible than any of TMIV, IX or XI (69, 103, 120). Three of the mutants (at amino acids Asn227, Ile233, Leu243) were greatly inhibited by MTSET, while 7 others were inhibited to a lesser degree. A positive control, Phe161 of TMIV, was inhibited by both MTSES and MTSET. In no cases did reactivity with MTSES cause any inhibition with the amino acids of TMVI. The

cysteine mutants of TMVI treated with MTSES either yielded 100% control activity or minor increases in pH recovery. There are two possible explanations for this: first, MTSES is repelled by the negatively charged residues located at the pore and near the pore openings, such that MTSES cannot access and modify TMVI cysteine mutants; second, modification of cysteine mutants by MTSES has no effect on cation translocation. Overall, TMVI cysteine mutants were much more susceptible to MTSET compared to MTSES. We suggest that the bulky trimethyl-ammonium and positive charge on MTSET have more impact on NHE1 cation translocation. Na^+ and H^+ ions may be electrostatically repelled or blocked by the MTSET modified cysteine side chain. On the other hand, there is insufficient evidence to imply that MTSET and MTSES do not modify cysteine mutants that exhibit normal activities. These results suggest that many residues of TMVI are pore lining and that this segment plays an important role in forming the pore of the NHE1 protein. While the residues strongly inhibited by MTSET (Asn227, Ile233 and Leu243) are compelling candidates for pore lining residues, those partially inhibited (Phe230, Gly231, Ala236, Val237, Ala244, Val 245 and Glu248) are less defined. Residues Ala244 and Val245 are next to Leu243 and may have partial access to the pore. We have previously found a similar phenomenon in TMIX, residues adjacent to strongly inhibited residues were also tended to be partially inhibited (103).

The structure of TMVI was determined earlier by our laboratory in collaboration with Dr. Sykes laboratory (128). Figure 15 illustrates the structure of TMVI segment in DPC micelles and highlighting the MTSET reactive residues

in N- and C-terminals. TMVI is a discontinuous helix segment with a flexible loop in the center linking two short alpha helices (Leu229 – Ala236 and Pro239 – Ile249). The flexible region contains a Pro239; proline residues are often observed in kinks and are regarded as helix breakers (9). Such distortion in TM segment is commonly observed in transporters and channels, and it is often functionally critical (54). The cation transport activity, protein expression, and surface localization of Pro239Cys mutant were significantly reduced. In addition, the cysteine mutation of Pro239 resulted in expression of premature NHE1. This indicates that Pro239 of TMVI is especially important in NHE1 processing. The Asp238-Pro239-Val240 (DPV) sequence of TMVI is highly conserved among the NHE isoforms and yeast Na^+/H^+ exchanger SOD2 (85). All three residues upstream of Pro239 (Ala236, Val237 and Asp238) were important in activity or expression and when substituted to cysteine, the mutations resulted in decreases in NHE1 activity. Moreover the A236C and V237C mutants were partially inhibited by reactivity with MTSET, suggesting they are accessible from the cell exterior and pore lining or at least partially accessible to the pore. This extended region (Val237 – Asp238) of the TMVI segment appears to be critical to NHE1 function. The loop allows flexible movements in the segment and contributes to the dynamic structure of NHE1 pore. MTSET reactive residues in the N-terminal, Asn227, Phe230, Ile233, Ala236 and Val237 align along a similar face, that is perhaps pore lining. While the residues Ala244, Val245 and Glu248 line up on the same face of the C-terminal helix, they do not align with the N-terminal MTSET reactive residues, though it must be remembered they are separated by an

extended flexible region. The side chain Leu243 does not seem to align well with the rest of MTSET sensitive residues, however we need to keep in mind that the TM segment is likely to take altered positions in different states of the transport cycle. It is unknown how the pore lining segments change their conformations. Paramagnetic relaxation experiments acquired information on the interaction between TMVI peptide and DPC micelle, and determined the solvent accessible face of TMVI (128). Interestingly, Mn^{2+} accessible residues such as Gly231, Ala236, Asp238, Ala244, and Glu247 were also either partially inhibited by MTSET or expressed inactive NHE1 when substituted to cysteine.

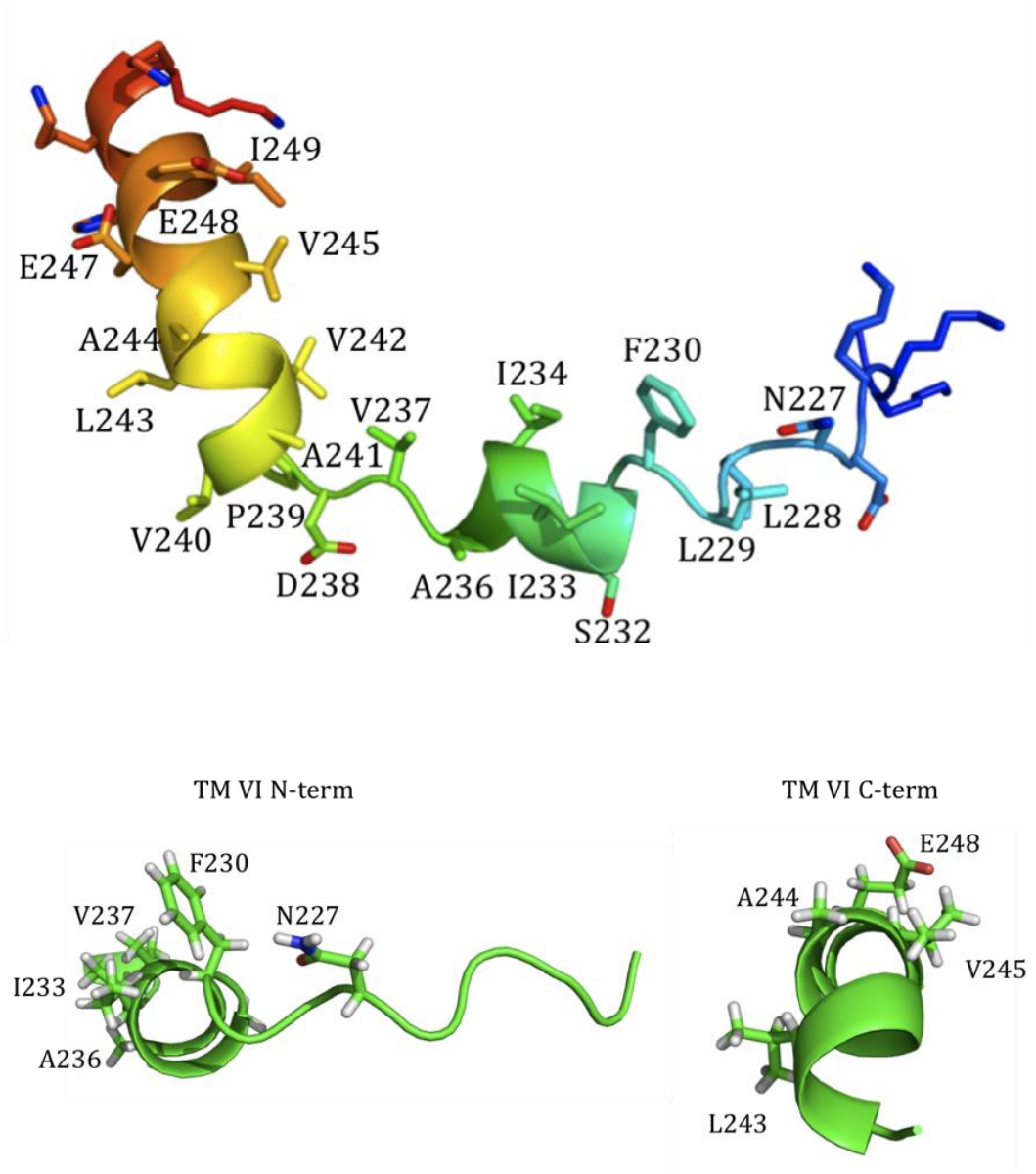

Figure 15. NMR structures of NHE1 TMVI. The NMR structure of TMVI peptide (D226 – H250) was determined by Brian Lee. The peptide is a discontinuous helix with a flexible loop in the segment center. Viewing the N-terminal segment of TMVI peptide revealed the alignment of side chains from critical residues. TMVI C-terminal segment also displayed the side chains of critical residues facing in a similar direction (128).

4.3 Functions of critical residues of TMVI

Further investigation of TMVI critical residues revealed their possible roles in NHE1. Asn227 was substituted to Ala, Asp, and Arg. Ile233 and Leu243 were mutated to Ala and Glu247 and Glu248 were mutated to Asp and Gln. The activities of Asn227Ala, Asn227Asp, and Asn227Arg were significantly reduced to 74%, 40% and 7% of wild type activity respectively. Asn contains an uncharged polar side chain, and substitution to alanine had the least effect on NHE1 activity. When Asn227 was mutated into Asp, which is a negatively charged residue, the activity of NHE1 dropped to 40% of control. Substituting Arg, a positively charged amino acid, for Asn227 seemed to be the most unfavorable. This mutation lead to expression of only the immature form of NHE1 with an activity of 7% on wild type NHE1 control. These results indicate that Asn227 is required for normal NHE1 expression and activity. None of the mutations in Asn227 was well tolerated; Asn227Cys and Asn227Arg expressed reduced amounts of NHE1 and only the immature form of NHE1 respectively. Asn227Ala and Asn227Asp exhibited diminished NHE1 activity but expressed and targeted normal amounts of protein. Asn227 is clearly a critical amino acid. Results with cysteine scanning mutagenesis show that it is pore lining. Mutation to other residues show that change to other amino acids can affect expression levels and targeting, and also affect NHE1 activity independent of these effects. Mutation of Asn227 to Arg is most unfavorable because of the positive charge. This positive charge could affect both cation coordination, or perhaps cause destabalization of other balancing electrostatic forces within the membrane. This

could lead to conformational changes in the protein which led to loss of production of the fully glycosylated protein.

Substitution of Ile233 and Leu243 to alanine led to reduced NHE1 expression at 45% and 86% control levels respectively. Ile233Cys and Ile233Ala mutations both expressed NHE1 at very low levels indicating their importance in regulating NHE1 expression. Both mutants Ile233Ala and Leu243Ala exhibited a significant reduction of activity at ~6% of control. These results demonstrate that these amino acids are not only pore lining, but there side chain is critical to the maintenance of NHE1 activity. Overall, the three most sensitive MTSET pore lining residues, Asn227, Ile233, and Leu243 are highly sensitive to mutation to other amino acids.

Glu247Gln and Glu248Asp mutants exhibited no reduction in their cation exchange activity and they had wild type protein expression and surface localization. In contrast, Glu247Asp and Glu248Gln mutants were reduced to 42% and 35% of control activities, without appreciable changes in expression levels and targeting. In the case of Glu247, the mutation to Gln demonstrates that the carboxyl is not required at this position of NHE1 activity. However the size of the side chain appears more critical as mutation to Asp greatly reduced activity. On the other hand, the negative charge on Glu248 is important for normal NHE1 activity. When Glu248 was substituted to Gln, the activity reduced to 35% even though it had normal protein expression and surface localization levels. These results suggest that Glu247 might play more of a role in maintaining structural requirements while Glu248 could be more critical in cation transport or in the

formation of intermolecular bonds with other transmembrane segments, through its charged carboxyl side chain.

To further understand the nature of the defects in the NHE1 protein, we examined the effects of the mutations Ile233Ala, Leu243Ala, Glu247Asp, and Glu248Gln on the conformation of NHE1. Limited digestion with trypsin was used to determine if a conformational change had occurred (86). The results are shown in Figure 14 where the digestion patterns of WT NHE1 and mutant proteins are compared with varying amounts of trypsin:protein. As the trypsin:protein ratio decreases, the degree of digestion declines. At a dilution of 1:3000, most of the WT NHE1 protein remained intact. Glu247Asp and Ile233Ala exhibited no significant difference in degradation patterns. In the Glu248Gln mutant, NHE1 was much more susceptible to trypsin in comparison to WT NHE1. At even the lowest trypsin to protein ratio, most of the NHE1 protein was degraded. At higher trypsin concentrations, virtually all of the Glu248Gln protein was degraded while much of the wild type protein remained. In the case of the Leu243Ala mutant protein, there appeared to be a slight increase in susceptibility to trypsin compared with WT NHE1. Overall, the degradation patterns of Glu248Gln and Leu243Ala suggest that these residues may be important in protein conformation. Our results cannot exclude that a conformational change occurs in the Glu247Asp mutant. Our assay was dependent on detection of changes in conformation of NHE1 using an antibody against the HA-tag on the protein. A change that affected conformation but not susceptibility to proteolysis, would not be detected. Nevertheless, we were able to

demonstrate that conformation changes occurred in the Glu248Gln and the Leu243Ala mutant proteins that made them more susceptible to proteolysis. In the case of the Glu248Gln mutant, there appears to be a large change in conformation.

Figure 16 depicts a model of the TMVI/XI assembly which is derived from homology structural model of EcNhaA (67). Amino acids of TMVI and TMXI that are pore lining and critical for cation transport are indicated. Asp238 is situated between the assembly of discontinuous helices TMVI/XI, and it compensates for the positive polarity contributed by the N-terminal ends. Supporting this concept are our results that showed that mutation of this amino acid to cysteine eliminated activity. In addition, the Pro239Cys mutant was also inactive. Neighboring residues of Asp238 and Pro239, were also pore lining (Ala236 and Val237). In between the C-terminal negative polarities of TMVI/XI assembly lies an Arg425 compensating for the negative charge. The putative protonation site Asp267 is also shown in the diagram, where it is located in close proximity to the pore lining residues of Ile233 and Ala236 in TMVI, and Ile461 and Leu465 in TMXI (69, 128). Ile233, Ala236, Ile461, and Leu465 cysteine mutants were shown to be susceptible to MTSET treatment, which led to decreased activity (69). This supports the idea that MTSET modification on these pore lining residues with side chains facing the closely situated putative protonation site Asp267 affect cation transport.

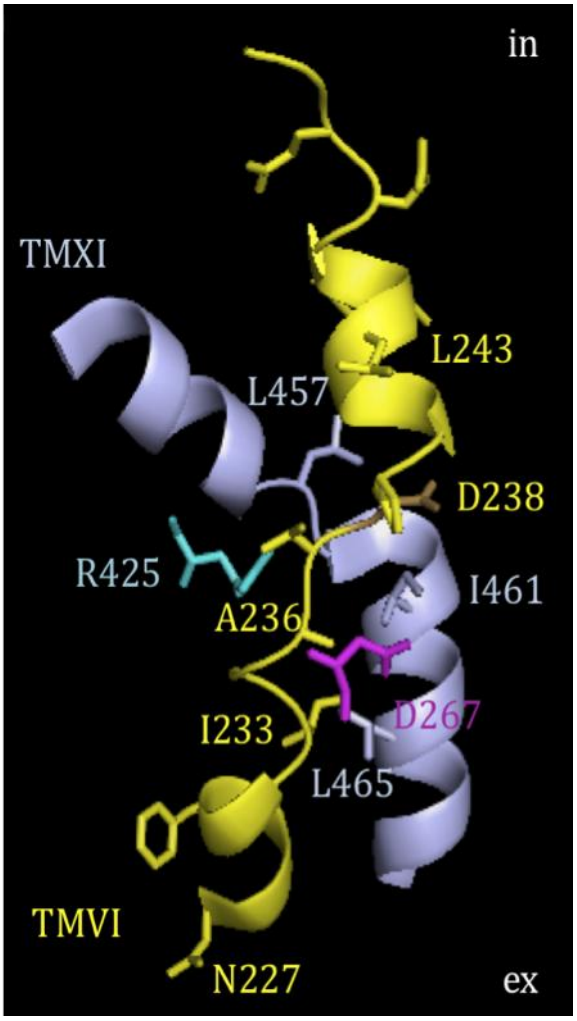

Figure 16. TMVI/TMXI assembly based on Landau's homology model structure of NHE1. The amino acid side chains of pore lining residues of TMVI (yellow) and TMXI (light blue) are shown**.** R425 (cyan) from TMX and D267 (pink) from TMVII are important cation translocation residues that are also illustrated (67, 69).

4.4 Summary

Overall, our results have shown that TMVI (amino acids 227-249) is a pore lining TM segment that is critical to NHE1 function. Application of cysteine scanning mutagenesis determined which residues are pore lining residues. Asn227, Ile233, and Leu243 mutations to cysteine exhibited the greatest inhibition by MTSET treatment. Several residues, Phe230, Gly231, Ala236, Val237, Ala244, Val245, and Glu248, were slightly inhibited by MTSET treatment. The positive charge and bulky trimethyl-ammonium group of MTSET contributed to activity inhibition. None of the TM VI cysteine mutants were affected by MTSES suggesting that introduction of a positive charge might be inhibitory to cation translocation.

The pore lining residues in TMVI were highly susceptible to single amino acid substitution mutagenesis. Substituting Asn227 to Cys and Arg decreased the amount of mature NHE1 protein expression; Asn227 mutation to Asp and Ala reduced the activity of NHE1. Mutations in Ile233 diminished NHE1 protein expression and activity drastically. Leu243Cys and Leu243Ala mutants also exhibited low cation exchange activity.

Limited trypsin digestion of TM VI mutants suggests that Leu243 and Glu248 residues are important in NHE1 protein folding and stability. Mutations of Leu243Ala and Glu248Gln produced notable degradation pattern differences from controls, revealing changes in protein conformation that caused susceptibility to trypsin proteolytic attack.

4.4 Future studies

A variety of approaches can be used to shed more information on the mammalian NHE1 protein and the mechanism of transport of cations by this membrane protein.

I. Resolving the whole length high resolution crystal structure of NHE1 is critical for the understanding of NHE1 mechanism. Not only the cation translocation steps can be revealed, but the binding sites for regulatory proteins could also be examined.

II. Given that achieving a crystal structure of mammalian NHE1 may be difficult, an alternative procedure is the determination of the structure of NHE1 transmembrane segments and loops by NMR spectroscopy. By assembling NMR segments structures, one can produce a full length structure of NHE1. The NMR structures of proteins are comparable to their crystal structures (59, 81, 104).

III. Determine the topology that best represents the real form of NHE1 in plasma membrane. Two topologies of NHE1 have been suggested, and they have different transmembrane segment assignments (67, 132). One major difference between the two topologies is the assignment of the first two transmembrane segments. Landau suggested that a part of the N-terminal segment in NHE1 is cleaved as signal peptide. Therefore the first TM in Landau's model begins at Val129, whereas in Wakabayashi's model TMI begins at His13. Applying mass spectrometry to a trypsinized sample of NHE1 excised from SDS-PAGE gel, one can perhaps detect the presence of the first two TM segment peptide fragments. Another method to investigate the topology of NHE1, is to introduce cysteine

mutations in TM9 (374 – 398 aa) of Landau's model and look at the accessibility of sulfhydryl reactive compounds. This segment is assigned as a re-entrant loop in Wakabayashi's model, where it was investigated previously to contain two residues that were inaccessible to biotin-maleimide from both extracellular and intracellular sides (132).

IV. Investigate the function of Asp238 in NHE1 to unravel its helix dipole compensation properties. Substitute Asp238 to a similarly charged Glu, an uncharged polar Asn, and a positively charged Arg and assess their activities. I postulate that substituting Asp238 to Arg will have the most detrimental effects on stabilizing the positively charged helix dipoles.

Chapter V

References

1. Aharonovitz O, Demaurex N, Woodside M, and Grinstein S. ATP dependence is not an intrinsic property of Na^+/H^+ exchanger NHE1: requirement for an ancillary factor. *Am J Physiol* 276: C1303-1311, 1999.

2. Aharonovitz O, Zaun HC, Balla T, York JD, Orlowski J, and Grinstein S. Intracellular pH regulation by Na^+/H^+ exchange requires phosphatidylinositol 4,5-bisphosphate. *J Cell Biol* 150: 213-224, 2000.

3. Alexander RT and Grinstein S. Tethering, recycling and activation of the epithelial sodium-proton exchanger, NHE3. *J Exp Biol* 212: 1630-1637, 2009.

4. Anderson SE, Kirkland DM, Beyschau A, and Cala PM. Acute effects of 17beta-estradiol on myocardial pH, Na^+, and Ca^{2+} and ischemia-reperfusion injury. *Am J Physiol Cell Physiol* 288: C57-64, 2005.

5. Aronson PS. Role of ion exchangers in mediating NaCl transport in the proximal tubule. *Kidney Int* 49: 1665-1670, 1996.

6. Attaphitaya S, Park K, and Melvin JE. Molecular cloning and functional expression of a rat Na^+/H^+ exchanger (NHE5) highly expressed in brain. *J Biol Chem* 274: 4383-4388, 1999.

7. Avkiran M, Gross G, Karmazyn M, Klein H, Murphy E, and Ytrehus K. Na^+/H^+ exchange in ischemia, reperfusion and preconditioning. *Cardiovasc Res* 50: 162-166, 2001.

8. Baird NR, Orlowski J, Szabo EZ, Zaun HC, Schultheis PJ, Menon AG, and Shull GE. Molecular cloning, genomic organization, and functional expression of Na^+/H^+ exchanger isoform 5 (NHE5) from human brain. *J Biol Chem* 274: 4377-4382, 1999.

9. Barlow DJ and Thornton JM. Helix geometry in proteins. *J Mol Biol* 201: 601-619, 1988.

10. Bell SM, Schreiner CM, Schultheis PJ, Miller ML, Evans RL, Vorhees CV, Shull GE, and Scott WJ. Targeted disruption of the murine Nhe1 locus induces ataxia, growth retardation, and seizures. *Am J Physiol* 276: C788-795, 1999.

11. Bertrand B, Wakabayashi S, Ikeda T, Pouyssegur J, and Shigekawa M. The Na^+/H^+ exchanger isoform 1 (NHE1) is a novel member of the calmodulin-binding proteins. Identification and characterization of calmodulin-binding sites. *J Biol Chem* 269: 13703-13709, 1994.

12. Bookstein C, Xie Y, Rabenau K, Musch MW, McSwine RL, Rao MC, and Chang EB. Tissue distribution of Na^+/H^+ exchanger isoforms NHE2 and NHE4 in rat intestine and kidney. *Am J Physiol* 273: C1496-1505, 1997.

13. Brant SR, Yun CH, Donowitz M, and Tse CM. Cloning, tissue distribution, and functional analysis of the human Na^+/H^+ exchanger isoform, NHE3. *Am J Physiol* 269: C198-206, 1995.

14. Brett CL, Donowitz M, and Rao R. Evolutionary origins of eukaryotic sodium/proton exchangers. *Am J Physiol Cell Physiol* 288: C223-239, 2005.

15. Casey JR, Grinstein S, and Orlowski J. Sensors and regulators of intracellular pH. *Nat Rev Mol Cell Biol* 11: 50-61.

16. Chambrey R, Achard JM, and Warnock DG. Heterologous expression of rat NHE4: a highly amiloride-resistant Na^+/H^+ exchanger isoform. *Am J Physiol* 272: C90-98, 1997.

17. Chen L, Gan XT, Haist JV, Feng Q, Lu X, Chakrabarti S, and Karmazyn M. Attenuation of compensatory right ventricular hypertrophy and heart failure following monocrotaline-induced pulmonary vascular injury by the Na^+-H^+ exchange inhibitor cariporide. *J Pharmacol Exp Ther* 298: 469-476, 2001.

18. Counillon L, Franchi A, and Pouyssegur J. A point mutation of the Na^+/H^+ exchanger gene (NHE1) and amplification of the mutated allele confer amiloride resistance upon chronic acidosis. *Proc Natl Acad Sci U S A* 90: 4508-4512, 1993.

19. Counillon L, Noel J, Reithmeier RA, and Pouyssegur J. Random mutagenesis reveals a novel site involved in inhibitor interaction within the fourth transmembrane segment of the Na^+/H^+ exchanger-1. *Biochemistry* 36: 2951-2959, 1997.

20. Counillon L, Pouyssegur J, and Reithmeier RA. The Na^+/H^+ exchanger NHE-1 possesses N- and O-linked glycosylation restricted to the first N-terminal extracellular domain. *Biochemistry* 33: 10463-10469, 1994.

21. Daniel H. Molecular and integrative physiology of intestinal peptide transport. *Annu Rev Physiol* 66: 361-384, 2004.

22. Demaurex N. pH Homeostasis of cellular organelles. *News Physiol Sci* 17: 1-5, 2002.

23. Demaurex N and Grinstein S. Na^+/H^+ antiport: modulation by ATP and role in cell volume regulation. *J Exp Biol* 196: 389-404, 1994.

24. Denker SP and Barber DL. Cell migration requires both ion translocation and cytoskeletal anchoring by the Na-H exchanger NHE1. *J Cell Biol* 159: 1087-1096, 2002.

25. Denker SP, Huang DC, Orlowski J, Furthmayr H, and Barber DL. Direct binding of the Na--H exchanger NHE1 to ERM proteins regulates the cortical cytoskeleton and cell shape independently of H^+ translocation. *Mol Cell* 6: 1425-1436, 2000.

26. Diering GH, Church J, and Numata M. Secretory Carrier Membrane Protein 2 Regulates Cell-surface Targeting of Brain-enriched Na^+/H^+ Exchanger NHE5. *J Biol Chem* 284: 13892-13903, 2009.

27. Ding J, Ng RW, and Fliegel L. Functional characterization of the transmembrane segment VII of the NHE1 isoform of the Na^+/H^+ exchanger. *Can J Physiol Pharmacol* 85: 319-325, 2007.

28. Ding J, Rainey JK, Xu C, Sykes BD, and Fliegel L. Structural and functional characterization of transmembrane segment VII of the Na^+/H^+ exchanger isoform 1. *J Biol Chem* 281: 29817-29829, 2006.

29. Engelhardt S, Hein L, Keller U, Klambt K, and Lohse MJ. Inhibition of Na^+-H^+ exchange prevents hypertrophy, fibrosis, and heart failure in beta(1)-adrenergic receptor transgenic mice. *Circ Res* 90: 814-819, 2002.

30. Fafournoux P, Noel J, and Pouyssegur J. Evidence that Na^+/H^+ exchanger isoforms NHE1 and NHE3 exist as stable dimers in membranes with a high degree of specificity for homodimers. *J Biol Chem* 269: 2589-2596, 1994.

31. Fatehi M and Linsdell P. Novel residues lining the CFTR chloride channel pore identified by functional modification of introduced cysteines. *J Membr Biol* 228: 151-164, 2009.

32. Fliegel L. Molecular biology of the myocardial Na^+/H^+ exchanger. *J Mol Cell Cardiol* 44: 228-237, 2008.

33. Fliegel L. The Na^+/H^+ exchanger isoform 1. *Int J Biochem Cell Biol* 37: 33-37, 2005.

34. Ford P, Rivarola V, Kierbel A, Chara O, Blot-Chabaud M, Farman N, Parisi M, and Capurro C. Differential role of Na^+/H^+ exchange isoforms NHE-1 and NHE-2 in a rat cortical collecting duct cell line. *J Membr Biol* 190: 117-125, 2002.

35. Gawenis LR, Greeb JM, Prasad V, Grisham C, Sanford LP, Doetschman T, Andringa A, Miller ML, and Shull GE. Impaired gastric acid secretion in mice with a targeted disruption of the NHE4 Na^+/H^+ exchanger. *J Biol Chem* 280: 12781-12789, 2005.

36. Grenier AL, Abu-ihweij K, Zhang G, Ruppert SM, Boohaker R, Slepkov ER, Pridemore K, Ren JJ, Fliegel L, and Khaled AR. Apoptosis-induced alkalinization by the Na^+/H^+ exchanger isoform 1 is mediated through phosphorylation of amino acids Ser726 and Ser729. *Am J Physiol Cell Physiol* 295: C883-896, 2008.

37. Grinstein S, Woodside M, Waddell TK, Downey GP, Orlowski J, Pouyssegur J, Wong DC, and Foskett JK. Focal localization of the NHE-1 isoform of the Na^+/H^+ antiport: assessment of effects on intracellular pH. *EMBO J* 12: 5209-5218, 1993.

38. Harguindey S, Orive G, Luis Pedraz J, Paradiso A, and Reshkin SJ. The role of pH dynamics and the Na^+/H^+ antiporter in the etiopathogenesis and treatment of cancer. Two faces of the same coin--one single nature. *Biochim Biophys Acta* 1756: 1-24, 2005.

39. Haworth RS, Frohlich O, and Fliegel L. Multiple carbohydrate moieties on the Na^+/H^+ exchanger. *Biochem J* 289 (Pt 3): 637-640, 1993.

40. He B, Deng C, Zhang M, Zou D, and Xu M. Reduction of intracellular pH inhibits the expression of VEGF in K562 cells after targeted inhibition of the Na^+/H^+ exchanger. *Leuk Res* 31: 507-514, 2007.

41. He P and Yun CC. Mechanisms of the regulation of the intestinal Na^+/H^+ exchanger NHE3. *J Biomed Biotechnol* 2010: 238080.

42. Herz K, Rimon A, Olkhova E, Kozachkov L, and Padan E. Transmembrane segment II of NhaA Na^+/H^+ antiporter lines the cation passage, and Asp65 is critical for pH activation of the antiporter. *J Biol Chem* 285: 2211-2220.

43. Hisamitsu T, Ben Ammar Y, Nakamura TY, and Wakabayashi S. Dimerization is crucial for the function of the Na^+/H^+ exchanger NHE1. *Biochemistry* 45: 13346-13355, 2006.

44. Hisamitsu T, Pang T, Shigekawa M, and Wakabayashi S. Dimeric interaction between the cytoplasmic domains of the Na^+/H^+ exchanger NHE1 revealed by symmetrical intermolecular cross-linking and selective co-immunoprecipitation. *Biochemistry* 43: 11135-11143, 2004.

45. Hunte C, Screpanti E, Venturi M, Rimon A, Padan E, and Michel H. Structure of a Na^+/H^+ antiporter and insights into mechanism of action and regulation by pH. *Nature* 435: 1197-1202, 2005.

46. Ikeda T, Schmitt B, Pouyssegur J, Wakabayashi S, and Shigekawa M. Identification of cytoplasmic subdomains that control pH-sensing of the Na^+/H^+ exchanger (NHE1): pH-maintenance, ATP-sensitive, and flexible loop domains. *J Biochem* 121: 295-303, 1997.

47. Imahashi K, Mraiche F, Steenbergen C, Murphy E, and Fliegel L. Overexpression of the Na^+/H^+ exchanger and ischemia-reperfusion injury in the myocardium. *Am J Physiol Heart Circ Physiol* 292: H2237-2247, 2007.

48. Ives HE and Rector FC, Jr. Proton transport and cell function. *J Clin Invest* 73: 285-290, 1984.

49. Jandeleit-Dahm K, Hannan KM, Farrelly CA, Allen TJ, Rumble JR, Gilbert RE, Cooper ME, and Little PJ. Diabetes-induced vascular hypertrophy is accompanied by activation of Na^+-H^+ exchange and prevented by Na^+-H^+ exchange inhibition. *Circ Res* 87: 1133-1140, 2000.

50. Javadpour MM, Eilers M, Groesbeek M, and Smith SO. Helix packing in polytopic membrane proteins: role of glycine in transmembrane helix association. *Biophys J* 77: 1609-1618, 1999.

51. Jessen F, Sjoholm C, and Hoffmann EK. Identification of the anion exchange protein of Ehrlich cells: a kinetic analysis of the inhibitory effects of 4,4'-diisothiocyano-2,2'-stilbene-disulfonic acid (DIDS) and labeling of membrane proteins with 3H-DIDS. *J Membr Biol* 92: 195-205, 1986.

52. Karmazyn M, Liu Q, Gan XT, Brix BJ, and Fliegel L. Aldosterone increases NHE-1 expression and induces NHE-1-dependent hypertrophy in neonatal rat ventricular myocytes. *Hypertension* 42: 1171-1176, 2003.

53. Kato Y, Lambert CA, Colige AC, Mineur P, Noel A, Frankenne F, Foidart JM, Baba M, Hata R, Miyazaki K, and Tsukuda M. Acidic extracellular pH induces matrix metalloproteinase-9 expression in mouse metastatic melanoma cells through the phospholipase D-mitogen-activated protein kinase signaling. *J Biol Chem* 280: 10938-10944, 2005.

54. Kauko A, Illergard K, and Elofsson A. Coils in the membrane core are conserved and functionally important. *J Mol Biol* 380: 170-180, 2008.

55. Kemp G, Young H, and Fliegel L. Structure and function of the human Na^+/H^+ exchanger isoform 1. *Channels (Austin)* 2, 2008.

56. Khadilkar A, Iannuzzi P, and Orlowski J. Identification of sites in the second exomembrane loop and ninth transmembrane helix of the mammalian Na+/H+ exchanger important for drug recognition and cation translocation. *J Biol Chem* 276: 43792-43800, 2001.

57. Klein M, Seeger P, Schuricht B, Alper SL, and Schwab A. Polarization of Na^+/H^+ and Cl^-/HCO_3^- exchangers in migrating renal epithelial cells. *J Gen Physiol* 115: 599-608, 2000.

58. Koblinski JE, Ahram M, and Sloane BF. Unraveling the role of proteases in cancer. *Clin Chim Acta* 291: 113-135, 2000.

59. Kresimir Sikic ST, and Oliviero Carugo. Systematic Comparison of Crystal and NMR Protein Structures Deposited in the Protein Data Bank. *The Open Biochemistry Journal* 4: 83-95, 2010.

60. Krulwich TA. Na^+/H^+ antiporters. *Biochim Biophys Acta* 726: 245-264, 1983.

61. Krump E, Nikitas K, and Grinstein S. Induction of tyrosine phosphorylation and Na^+/H^+ exchanger activation during shrinkage of human neutrophils. *J Biol Chem* 272: 17303-17311, 1997.

62. Kyte J and Doolittle RF. A simple method for displaying the hydropathic character of a protein. *J Mol Biol* 157: 105-132, 1982.

63. Lacroix J, Poet M, Huc L, Morello V, Djerbi N, Ragno M, Rissel M, Tekpli X, Gounon P, Lagadic-Gossmann D, and Counillon L. Kinetic analysis of the regulation of the Na^+/H^+ exchanger NHE-1 by osmotic shocks. *Biochemistry* 47: 13674-13685, 2008.

64. Lacroix J, Poet M, Maehrel C, and Counillon L. A mechanism for the activation of the Na/H exchanger NHE-1 by cytoplasmic acidification and mitogens. *EMBO Rep* 5: 91-96, 2004.

65. Ladoux A, Miglierina R, Krawice I, Cragoe EJ, Jr., Abita JP, and Frelin C. Single-cell analysis of the intracellular pH and its regulation during the monocytic differentiation of U937 human leukemic cells. *Eur J Biochem* 175: 455-460, 1988.

66. Lagarde AE, Franchi AJ, Paris S, and Pouyssegur JM. Effect of mutations affecting Na^+: H^+ antiport activity on tumorigenic potential of hamster lung fibroblasts. *J Cell Biochem* 36: 249-260, 1988.

67. Landau M, Herz K, Padan E, and Ben-Tal N. Model structure of the Na^+/H^+ exchanger 1 (NHE1): functional and clinical implications. *J Biol Chem* 282: 37854-37863, 2007.

68. Le Gall M, Grall D, Chambard JC, Pouyssegur J, and Van Obberghen-Schilling E. An anchorage-dependent signal distinct from p42/44 MAP kinase activation is required for cell cycle progression. *Oncogene* 17: 1271-1277, 1998.

69. Lee BL, Li X, Liu Y, Sykes BD, and Fliegel L. Structural and functional analysis of transmembrane XI of the NHE1 isoform of the Na^+/H^+ exchanger. *J Biol Chem* 284: 11546-11556, 2009.

70. Lee SH, Kim T, Park ES, Yang S, Jeong D, Choi Y, and Rho J. NHE10, an osteoclast-specific member of the Na^+/H^+ exchanger family, regulates osteoclast differentiation and survival [corrected]. *Biochem Biophys Res Commun* 369: 320-326, 2008.

71. Lehoux S, Abe J, Florian JA, and Berk BC. 14-3-3 Binding to Na^+/H^+ exchanger isoform-1 is associated with serum-dependent activation of Na^+/H^+ exchange. *J Biol Chem* 276: 15794-15800, 2001.

72. Li X, Alvarez B, Casey JR, Reithmeier RA, and Fliegel L. Carbonic anhydrase II binds to and enhances activity of the Na^+/H^+ exchanger. *J Biol Chem* 277: 36085-36091, 2002.

73. Li X, Ding J, Liu Y, Brix BJ, and Fliegel L. Functional analysis of acidic amino acids in the cytosolic tail of the Na^+/H^+ exchanger. *Biochemistry* 43: 16477-16486, 2004.

74. Li X, Karki P, Lei L, Wang H, and Fliegel L. Na^+/H^+ exchanger isoform 1 facilitates cardiomyocyte embryonic stem cell differentiation. *Am J Physiol Heart Circ Physiol* 296: H159-170, 2009.

75. Li X, Liu Y, Alvarez BV, Casey JR, and Fliegel L. A novel carbonic anhydrase II binding site regulates NHE1 activity. *Biochemistry* 45: 2414-2424, 2006.

76. Mailander J, Muller-Esterl W, and Dedio J. Human homolog of mouse tescalcin associates with Na^+/H^+ exchanger type-1. *FEBS Lett* 507: 331-335, 2001.

77. Malakooti J, Dahdal RY, Schmidt L, Layden TJ, Dudeja PK, and Ramaswamy K. Molecular cloning, tissue distribution, and functional expression of the human Na^+/H^+ exchanger NHE2. *Am J Physiol* 277: G383-390, 1999.

78. Malo ME and Fliegel L. Physiological role and regulation of the Na^+/H^+ exchanger. *Can J Physiol Pharmacol* 84: 1081-1095, 2006.

79. McSwine RL, Musch MW, Bookstein C, Xie Y, Rao M, and Chang EB. Regulation of apical membrane Na^+/H^+ exchangers NHE2 and NHE3 in intestinal epithelial cell line C2/bbe. *Am J Physiol* 275: C693-701, 1998.

80. Miyazaki E, Sakaguchi M, Wakabayashi S, Shigekawa M, and Mihara K. NHE6 protein possesses a signal peptide destined for endoplasmic reticulum membrane and localizes in secretory organelles of the cell. *J Biol Chem* 276: 49221-49227, 2001.

81. Mohanty B, Serrano P, Pedrini B, Jaudzems K, Geralt M, Horst R, Herrmann T, Elsliger MA, Wilson IA, and Wuthrich K. Comparison of NMR and crystal structures for the proteins TM1112 and TM1367. *Acta Crystallogr Sect F Struct Biol Cryst Commun* 66: 1381-1392.

82. Moncoq K, Kemp G, Li X, Fliegel L, and Young HS. Dimeric structure of human Na^+/H^+ exchanger isoform 1 overproduced in Saccharomyces cerevisiae. *J Biol Chem* 283: 4145-4154, 2008.

83. Monod J, Wyman J, and Changeux JP. On the Nature of Allosteric Transitions: A Plausible Model. *J Mol Biol* 12: 88-118, 1965.

84. Murphy E, Cross HR, and Steenbergen C. Is Na/Ca exchange during ischemia and reperfusion beneficial or detrimental? *Ann N Y Acad Sci* 976: 421-430, 2002.

85. Murtazina R, Booth BJ, Bullis BL, Singh DN, and Fliegel L. Functional analysis of polar amino-acid residues in membrane associated regions of the NHE1 isoform of the mammalian Na+/H+ exchanger. *Eur J Biochem* 268: 4674-4685, 2001.

86. Nakamoto RK, Verjovski-Almeida S, Allen KE, Ambesi A, Rao R, and Slayman CW. Substitutions of aspartate 378 in the phosphorylation domain of the yeast PMA1 H+-ATPase disrupt protein folding and biogenesis. *J Biol Chem* 273: 7338-7344, 1998.

87. Nakamura N, Tanaka S, Teko Y, Mitsui K, and Kanazawa H. Four Na^+/H^+ exchanger isoforms are distributed to Golgi and post-Golgi compartments and are involved in organelle pH regulation. *J Biol Chem* 280: 1561-1572, 2005.

88. Ndayizeye M, Touret N, and Fliegel L. Proline 146 is critical to the structure, function and targeting of sod2, the Na^+/H^+ exchanger of Schizosaccharomyces pombe. *Biochim Biophys Acta* 1788: 983-992, 2009.

89. Nielsen H, Engelbrecht J, Brunak S, and von Heijne G. A neural network method for identification of prokaryotic and eukaryotic signal peptides and prediction of their cleavage sites. *Int J Neural Syst* 8: 581-599, 1997.

90. Nielsen H, Engelbrecht J, Brunak S, and von Heijne G. Identification of prokaryotic and eukaryotic signal peptides and prediction of their cleavage sites. *Protein Eng* 10: 1-6, 1997.

91. Orlov SN, Adarichev VA, Devlin AM, Maximova NV, Sun YL, Tremblay J, Dominiczak AF, Postnov YV, and Hamet P. Increased Na^+/H^+ exchanger isoform 1 activity in spontaneously hypertensive rats: lack of mutations within the coding region of NHE1. *Biochim Biophys Acta* 1500: 169-180, 2000.

92. Orlowski J and Grinstein S. Diversity of the mammalian sodium/proton exchanger SLC9 gene family. *Pflugers Arch* 447: 549-565, 2004.

93. Paletas K, Sailer X, Rizeq L, Dimitriadi A, Koliakos G, and Kaloyianni M. Angiotensin-II-dependent NHE1 activation in human monocytes. *J Am Soc Hypertens* 2: 173-181, 2008.

94. Pang T, Hisamitsu T, Mori H, Shigekawa M, and Wakabayashi S. Role of calcineurin B homologous protein in pH regulation by the Na+/H+ exchanger 1: tightly bound Ca2+ ions as important structural elements. *Biochemistry* 43: 3628-3636, 2004.

95. Pang T, Su X, Wakabayashi S, and Shigekawa M. Calcineurin homologous protein as an essential cofactor for Na^+/H^+ exchangers. *J Biol Chem* 276: 17367-17372, 2001.

96. Pang T, Wakabayashi S, and Shigekawa M. Expression of calcineurin B homologous protein 2 protects serum deprivation-induced cell death by serum-independent activation of Na^+/H^+ exchanger. *J Biol Chem* 277: 43771-43777, 2002.

97. Pedersen SF, King SA, Nygaard EB, Rigor RR, and Cala PM. NHE1 inhibition by amiloride- and benzoylguanidine-type compounds. Inhibitor binding loci deduced from chimeras of NHE1 homologues with endogenous differences in inhibitor sensitivity. *J Biol Chem* 282: 19716-19727, 2007.

98. Petrey D, Xiang Z, Tang CL, Xie L, Gimpelev M, Mitros T, Soto CS, Goldsmith-Fischman S, Kernytsky A, Schlessinger A, Koh IY, Alexov E, and Honig B. Using multiple structure alignments, fast model building, and energetic analysis in fold recognition and homology modeling. *Proteins* 53 Suppl 6: 430-435, 2003.

99. Piper HM, Meuter K, and Schafer C. Cellular mechanisms of ischemia-reperfusion injury. *Ann Thorac Surg* 75: S644-648, 2003.

100. Pizzonia JH, Biemesderfer D, Abu-Alfa AK, Wu MS, Exner M, Isenring P, Igarashi P, and Aronson PS. Immunochemical characterization of Na^+/H^+ exchanger isoform NHE4. *Am J Physiol* 275: F510-517, 1998.

101. Pouyssegur J, Chambard JC, Franchi A, Paris S, and Van Obberghen-Schilling E. Growth factor activation of an amiloride-sensitive Na^+/H^+ exchange system in quiescent fibroblasts: coupling to ribosomal protein S6 phosphorylation. *Proc Natl Acad Sci U S A* 79: 3935-3939, 1982.

102. Pouyssegur J, Sardet C, Franchi A, L'Allemain G, and Paris S. A specific mutation abolishing Na^+/H^+ antiport activity in hamster fibroblasts precludes growth at neutral and acidic pH. *Proc Natl Acad Sci U S A* 81: 4833-4837, 1984.

103. Reddy T, Ding J, Li X, Sykes BD, Rainey JK, and Fliegel L. Structural and functional characterization of transmembrane segment IX of the NHE1 isoform of the Na^+/H^+ exchanger. *J Biol Chem* 283: 22018-22030, 2008.

104. Reddy T, Li X, Fliegel L, Sykes BD, and Rainey JK. Correlating structure, dynamics, and function in transmembrane segment VII of the Na^+/H^+ exchanger isoform 1. *Biochim Biophys Acta* 1798: 94-104.

105. Reshkin SJ, Bellizzi A, Caldeira S, Albarani V, Malanchi I, Poignee M, Alunni-Fabbroni M, Casavola V, and Tommasino M. Na^+/H^+ exchanger-dependent intracellular alkalinization is an early event in malignant transformation and plays an essential role in the development of subsequent transformation-associated phenotypes. *FASEB J* 14: 2185-2197, 2000.

106. Reshkin SJ, Bellizzi A, Cardone RA, Tommasino M, Casavola V, and Paradiso A. Paclitaxel induces apoptosis via protein kinase A- and p38 mitogen-activated protein-dependent inhibition of the Na^+/H^+ exchanger (NHE) NHE isoform 1 in human breast cancer cells. *Clin Cancer Res* 9: 2366-2373, 2003.

107. Rich IN, Worthington-White D, Garden OA, and Musk P. Apoptosis of leukemic cells accompanies reduction in intracellular pH after targeted inhibition of the Na^+/H^+ exchanger. *Blood* 95: 1427-1434, 2000.

108. Rieder CV and Fliegel L. Transcriptional regulation of Na^+/H^+ exchanger expression in the intact mouse. *Mol Cell Biochem* 243: 87-95, 2003.

109. Rotin D and Grinstein S. Impaired cell volume regulation in Na^+-H^+ exchange-deficient mutants. *Am J Physiol* 257: C1158-1165, 1989.

110. Roxrud I, Raiborg C, Gilfillan GD, Stromme P, and Stenmark H. Dual degradation mechanisms ensure disposal of NHE6 mutant protein associated with neurological disease. *Exp Cell Res* 315: 3014-3027, 2009.

111. Rupprecht HJ, vom Dahl J, Terres W, Seyfarth KM, Richardt G, Schultheibeta HP, Buerke M, Sheehan FH, and Drexler H. Cardioprotective effects of the Na^+/H^+ exchange inhibitor cariporide in patients with acute anterior myocardial infarction undergoing direct PTCA. *Circulation* 101: 2902-2908, 2000.

112. Sardet C, Counillon L, Franchi A, and Pouyssegur J. Growth factors induce phosphorylation of the Na^+/H^+ antiporter, glycoprotein of 110 kD. *Science* 247: 723-726, 1990.

113. Sardet C, Franchi A, and Pouyssegur J. Molecular cloning, primary structure, and expression of the human growth factor-activatable Na^+/H^+ antiporter. *Cell* 56: 271-280, 1989.

114. Schultheis PJ, Clarke LL, Meneton P, Harline M, Boivin GP, Stemmermann G, Duffy JJ, Doetschman T, Miller ML, and Shull GE. Targeted disruption of the murine Na^+/H^+ exchanger isoform 2 gene causes reduced viability of gastric parietal cells and loss of net acid secretion. *J Clin Invest* 101: 1243-1253, 1998.

115. Shrode LD, Gan BS, D'Souza SJ, Orlowski J, and Grinstein S. Topological analysis of NHE1, the ubiquitous Na^+/H^+ exchanger using chymotryptic cleavage. *Am J Physiol* 275: C431-439, 1998.

116. Shugrue CA, Obermuller N, Bachmann S, Slayman CW, and Reilly RF. Molecular cloning of NHE3 from LLC-PK1 cells and localization in pig kidney. *J Am Soc Nephrol* 10: 1649-1657, 1999.

117. Slepkov E, Ding J, Han J, and Fliegel L. Mutational analysis of potential pore-lining amino acids in TM IV of the Na^+/H^+ exchanger. *Biochim Biophys Acta* 1768: 2882-2889, 2007.

118. Slepkov E and Fliegel L. Structure and function of the NHE1 isoform of the Na^+/H^+ exchanger. *Biochem Cell Biol* 80: 499-508, 2002.

119. Slepkov ER, Chow S, Lemieux MJ, and Fliegel L. Proline residues in transmembrane segment IV are critical for activity, expression and targeting of the Na^+/H^+ exchanger isoform 1. *Biochem J* 379: 31-38, 2004.

120. Slepkov ER, Rainey JK, Li X, Liu Y, Cheng FJ, Lindhout DA, Sykes BD, and Fliegel L. Structural and functional characterization of transmembrane segment IV of the NHE1 isoform of the Na^+/H^+ exchanger. *J Biol Chem* 280: 17863-17872, 2005.

121. Spacey SD, Szczygielski BI, McRory JE, Wali GM, Wood NW, and Snutch TP. Mutation analysis of the sodium/hydrogen exchanger gene (NHE5) in familial paroxysmal kinesigenic dyskinesia. *J Neural Transm* 109: 1189-1194, 2002.

122. Stock C and Schwab A. Role of the Na/H exchanger NHE1 in cell migration. *Acta Physiol (Oxf)* 187: 149-157, 2006.

123. Su X, Pang T, Wakabayashi S, and Shigekawa M. Evidence for involvement of the putative first extracellular loop in differential volume sensitivity of the Na^+/H^+ exchangers NHE1 and NHE2. *Biochemistry* 42: 1086-1094, 2003.

124. Szabo EZ, Numata M, Shull GE, and Orlowski J. Kinetic and pharmacological properties of human brain Na^+/H^+ exchanger isoform 5 stably expressed in Chinese hamster ovary cells. *J Biol Chem* 275: 6302-6307, 2000.

125. Theroux P, Chaitman BR, Danchin N, Erhardt L, Meinertz T, Schroeder JS, Tognoni G, White HD, Willerson JT, and Jessel A. Inhibition of the sodium-hydrogen exchanger with cariporide to prevent myocardial infarction in high-risk ischemic situations. Main results of the GUARDIAN trial. Guard during ischemia against necrosis (GUARDIAN) Investigators. *Circulation* 102: 3032-3038, 2000.

126. Thwaites DT and Anderson CM. H^+-coupled nutrient, micronutrient and drug transporters in the mammalian small intestine. *Exp Physiol* 92: 603-619, 2007.

127. Touret N, Poujeol P, and Counillon L. Second-site revertants of a low-sodium-affinity mutant of the Na^+/H^+ exchanger reveal the participation of TM4 into a highly constrained sodium-binding site. *Biochemistry* 40: 5095-5101, 2001.

128. Tzeng J, Lee BL, Sykes BD, and Fliegel L. Structural and functional analysis of transmembrane VI of the NHE1 isoform of the Na^+/H^+ exchanger. *J Biol Chem*.

129. Vexler ZS, Symons M, and Barber DL. Activation of Na+-H+ exchange is necessary for RhoA-induced stress fiber formation. *J Biol Chem* 271: 22281-22284, 1996.

130. Wakabayashi S, Hisamitsu T, Pang T, and Shigekawa M. Kinetic dissection of two distinct proton binding sites in Na^+/H^+ exchangers by measurement of reverse mode reaction. *J Biol Chem* 278: 43580-43585, 2003.

131. Wakabayashi S, Hisamitsu T, Pang T, and Shigekawa M. Mutations of Arg440 and Gly455/Gly456 oppositely change pH sensing of Na+/H+ exchanger 1. *J Biol Chem* 278: 11828-11835, 2003.

132. Wakabayashi S, Pang T, Su X, and Shigekawa M. A novel topology model of the human Na^+/H^+ exchanger isoform 1. *J Biol Chem* 275: 7942-7949, 2000.

133. Wakabayashi S, Pang T, Su X, and Shigekawa M. Second mutations rescue point mutant of the Na^+/H^+ exchanger NHE1 showing defective surface expression. *FEBS Lett* 487: 257-261, 2000.

134. Wang H, Singh D, and Fliegel L. The Na^+/H^+ antiporter potentiates growth and retinoic acid-induced differentiation of P19 embryonal carcinoma cells. *J Biol Chem* 272: 26545-26549, 1997.

135. West IC and Mitchell P. Proton/sodium ion antiport in Escherichia coli. *Biochem J* 144: 87-90, 1974.

136. Wuthrich K. Protein structure determination in solution by NMR spectroscopy. *J Biol Chem* 265: 22059-22062, 1990.

137. Yang N, George AL, Jr., and Horn R. Probing the outer vestibule of a sodium channel voltage sensor. *Biophys J* 73: 2260-2268, 1997.

138. Yang W, Dyck JR, and Fliegel L. Regulation of NHE1 expression in L6 muscle cells. *Biochim Biophys Acta* 1306: 107-113, 1996.

139. Yang X, Wang D, Dong W, Song Z, and Dou K. Inhibition of Na^+/H^+ exchanger 1 by 5-(N-ethyl-N-isopropyl) amiloride reduces hypoxia-induced hepatocellular carcinoma invasion and motility. *Cancer Lett* 295: 198-204.

140. Yu H, Freedman BI, Rich SS, and Bowden DW. Human Na^+/H^+ exchanger genes : identification of polymorphisms by radiation hybrid mapping and analysis of linkage in end-stage renal disease. *Hypertension* 35: 135-143, 2000.

141. Yu L, Quinn DA, Garg HG, and Hales CA. Deficiency of the NHE1 gene prevents hypoxia-induced pulmonary hypertension and vascular remodeling. *Am J Respir Crit Care Med* 177: 1276-1284, 2008.

142. Zizak M, Cavet ME, Bayle D, Tse CM, Hallen S, Sachs G, and Donowitz M. Na^+/H^+ exchanger NHE3 has 11 membrane spanning domains and a cleaved signal peptide: topology analysis using in vitro transcription/translation. *Biochemistry* 39: 8102-8112, 2000.

Appendix

Cell Line	% NHE1 on plasma membrane		
	total	glycosylated	unglycosylated
cNHE1 Ct	1.66 ± 3.7	0 ± 3.6	5.5 ± 3.0
WT NHE1	51.0 ± 1.8	67.3 ± 2.4	21.1 ± 3.1
cNHE1	53.6 ± 3.1	72.8 ± 3.3	17.9 ± 2.9
N227C	52.1 ± 3.4	67.4 ± 4.2	17.8 ± 4.6
L228C	41.8 ± 5.5	70.8 ± 4.1	9.2 ± 8.3
L229C	39.1 ± 1.6	$58.3 \pm 1.9^{+}$	5.0 ± 1.2
F230C	22.5 ± 1.8	62.4 ± 1.4	0 ± 2.3
G231C	34.9 ± 2.9	58.2 ± 2.9	8.3 ± 2.8
S232C	53.2 ± 1.5	78.0 ± 0.9	10.2 ± 1.9
I233C	48.8 ± 1.9	$87.3 \pm 1.9^{+}$	3.4 ± 4.1
I234C	35.5 ± 1.7	$58.8 \pm 1.7^{+}$	4.8 ± 1.0
S235C	27.0 ± 2.1	$44.0 \pm 2.1^{+}$	3.8 ± 3.1
A236C	52.4 ± 2.3	77.4 ± 2.1	13.1 ± 3.0
V237C	46.5 ± 1.0	74.3 ± 3.3	9.1 ± 1.1
D238C	42.3 ± 2.7	74.5 ± 2.0	2.9 ± 3.6
P239C	13.1 ± 4.3	0^{+}	13.1 ± 4.3
V240C	50.3 ± 1.7	78.0 ± 2.2	10.5 ± 2.3
A241C	32.8 ± 2.8	$45.6 \pm 4.0^{+}$	15.4 ± 2.8
V242C	42.9 ± 1.2	$57.9 \pm 0.9^{+}$	18.0 ± 1.2
L243C	48.3 ± 2.7	$84.9 \pm 2.1^{+}$	9.2 ± 3.4
A244C	41.1 ± 3.7	62.8 ± 5.7	6.7 ± 1.7
V245C	38.5 ± 3.4	$57.2 \pm 3.8^{+}$	8.2 ± 4.3
F246C	48.3 ± 6.7	66.4 ± 6.7	15.7 ± 6.6
E247C	10.6 ± 3.5	0^{+}	10.6 ± 3.5
E248C	42.8 ± 3.1	79.7 ± 2.2	13.7 ± 3.9
I249C	56.5 ± 3.3	78.6 ± 2.3	16.9 ± 2.8

Table 2. Summary of surface localization in total (glycosylated + unglycosylated), glycosylated (mature), and unglycosylated (immature) NHE1 TMVI cysteine mutants. $^{+}$ indicates significantly different surface localization of glycosylated NHE1 mutants than cNHE1 at $P<0.05$. Results are mean ± S.E. n = at least 6 experiments.

Cell Line	% NHE1 on plasma membrane		
	total	glycosylated	unglycosylated
WT NHE1	50.9 ± 2.4	60.0 ± 2.0	24.7 ± 4.5
N227A	41.4 ± 1.5	56.4 ± 2.0	3.9 ± 1.2
N227D	40.3 ± 4.6	66.9 ± 7.0	10.4 ± 3.8
N227R	5.3 ± 2.9	28.7 ± 5.4$^{\theta}$	1.0 ± 2.8
I233A	62.2 ± 5.2	85.1 ± 4.3$^{\theta}$	21.6 ± 5.1
L243A	45.3 ± 1.3	65.3 ± 1.0	8.9 ± 2.4
E247D	58.6 ± 3.1	64.7 ± 3.2	38.2 ± 4.1
E247Q	50.6 ± 2.1	61.5 ± 1.9	25.6 ± 2.7
E248D	36.4 ± 3.5	47.3 ± 3.9$^{\theta}$	11.0 ± 2.9
E248Q	61.0 ± 1.9	82.1 ± 1.6$^{\theta}$	17.4 ± 2.9

Table 3. Summary of surface localization in total (glycosylated + unglycosylated), glycosylated (mature), and unglycosylated (immature) NHE1 TMVI mutants. $^{\theta}$ indicates mutants with significantly different surface localization than cNHE1 at $P<0.05$. Results are mean +/- S.E. n = at least 6 experiments.

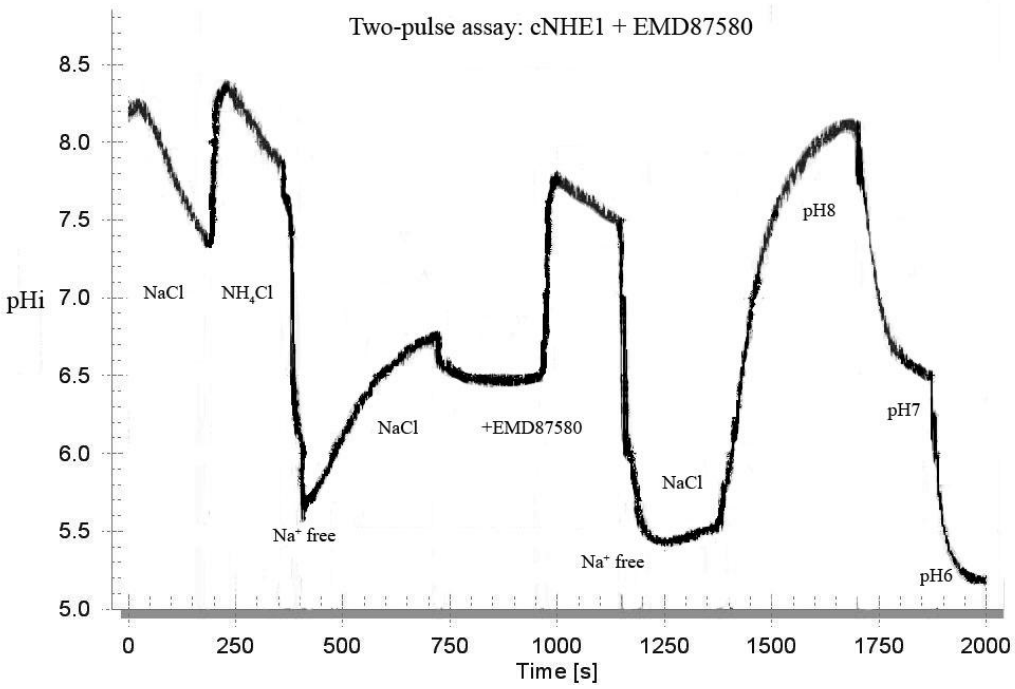

Figure 17. Two-pulse activity trace of cNHE1 with inhibitor EMD87580. Treatment of EMD87580 to cNHE1 abolished pH_i recovery after intracellular acidification by NH_4Cl. 10μM final concentration of EM87580 was added in assay buffers during the first recovery in normal buffer and through out the second acidification and recovery.